Chaudhry, F.A., Schmitz, D., Reimer, R.J., Larsson, P., Gray, A.T., Nicoll, R., Kavanaugh, M., Edwards, R.H., 2002. Glutamine uptake by neurons: interaction of protons with system a transporters. J. Neurosci 22 (1), 62–72.
Danbolt, N.C., 2001. Glutamate uptake. Prog. Neurobiol. 65 (1), 1–105.
Eybalin, M., Altschuler, R.A., 1990. Immunoelectron microscopic localization of neurotransmitters in the cochlea. J. Electron. Microsc. Tech. 15 (3), 209–224.
Eybalin, M., Norenberg, M.D., Renard, N., 1996. Glutamine synthetase and glutamate metabolism in the guinea pig cochlea. Hear. Res. 101 (1–2), 93–101.
Furness, D.N., Lawton, D.M., 2003. Comparative distribution of glutamate transporters and receptors in relation to afferent innervation density in the mammalian cochlea. J. Neurosci. 23 (36), 11296–11304.
Furness, D.N., Lehre, K.P., 1997. Immunocytochemical localization of a high-affinity glutamate-aspartate transporter, GLAST, in the rat and guinea-pig cochlea. Eur. J. Neurosci. 9 (9), 1961–1969.
Glowatzki, E., Cheng, N., Hiel, H., Yi, E., Tanaka, K., Ellis-Davies, G.C., Rothstein, J.D., Bergles, D.E., 2006. The glutamate-aspartate transporter GLAST mediates glutamate uptake at inner hair cell afferent synapses in the mammalian cochlea. J. Neurosci. 26 (29), 7659–7664.
Hakuba, N., Koga, K., Gyo, K., Usami, S.I., Tanaka, K., 2000. Exacerbation of noise-induced hearing loss in mice lacking the glutamate transporter GLAST. J. Neurosci. 20 (23), 8750–8753.
Hamdani, E.H., Gudbrandsen, M., Bjørkmo, M., Chaudhry, F.A., 2012. The system N transporter SN2 doubles as a transmitter precursor furnisher and a potential regulator of NMDA receptors, Glia, in press.
Jenstad, M., Quazi, A.Z., Zilberter, M., Haglerød, C., Berghuis, P., Saddique, N., Goiny, M., Buntup, D., Davanger, S., S. Haug, F.M., Barnes, C.A., McNaughton, B.L., Ottersen, O.P., Storm-Mathisen, J., Harkany, T., Chaudhry, F.A., 2009. System A transporter SAT2 mediates replenishment of dendritic glutamate pools controlling retrograde signaling by glutamate. Cereb. Cortex 19 (5), 1092–1106.
Mackenzie, B., Schäfer, M.K., Erickson, J.D., Hediger, M.A., Weihe, E., Varoqui, H., 2003. Functional properties and cellular distribution of the system A glutamine transporter SNAT1 support specialized roles in central neurons. J. Biol. Chem. 278 (26), 23720–23730.
Matsubara, A., Laake, J.H., Davanger, S., Usami, S., Ottersen, O.P., 1996. Organization of AMPA receptor subunits at a glutamate synapse: a quantitative immunogold analysis of hair cell synapses in the rat organ of Corti. J. Neurosci. 16 (14), 4457–4467.
Ottersen, O.P., Takumi, Y., Matsubara, A., Landsend, A.S., Laake, J.H., Usami, S., 1998. Molecular organization of a type of peripheral glutamate synapse: the afferent synapses of hair cells in the inner ear. Prog. Neurobiol. 54 (2), 127–148.
Robertson, D., 1983. Functional significance of dendritic swelling after loud sounds in the guinea pig cochlea. Hear. Res. 9 (3), 263–278.
Ruel, J., Emery, S., Nouvian, R., Bersot, T., Amilhon, B., Van Rybroek, J.M., Rebillard, G., Lenoir, M., Eybalin, M., Delprat, B., Sivakumaran, T.A., Giros, B., El Mestikawy, S., Moser, T., Smith, R.J., Lesperance, M.M., Puel, J.L., 2008. Impairment of SLC17A8 encoding vesicular glutamate transporter-3, VGLUT3, underlies nonsyndromic deafness DFNA25 and inner hair cell dysfunction in null mice. Am. J. Hum. Genet. 83 (2), 278–292.
Saunders, J.C., Dear, S.P., Schneider, M.E., 1985. The anatomical consequences of acoustic injury: a review and tutorial. J. Acoust. Soc. Am. 78 (3), 833–860.
Seal, R.P., Akil, O., Yi, E., Weber, C.M., Grant, L., Yoo, J., Clause, A., Kandler, K., Noebels, J.L., Glowatzki, E., Lustig, L.R., Edwards, R.H., 2008. Sensorineural deafness and seizures in mice lacking vesicular glutamate transporter 3. Neuron 57 (2), 263–275.
Solbu, T.T., Bjørkmo, M., Berghuis, P., Harkany, T., Chaudhry, F.A., 2010. SAT1, A Glutamine Transporter, is Preferentially Expressed in GABAergic Neurons. Front Neuroanat 4, 1.
Takumi, Y., Matsubara, A., Danbolt, N.C., Laake, J.H., Storm-Mathisen, J., Usami, S., Shinkawa, H., Ottersen, O.P., 1997. Discrete cellular and subcellular localization of glutamine synthetase and the glutamate transporter GLAST in the rat vestibular end organ. Neuroscience 79 (4), 1137–1144.
Takumi, Y., Matsubara, A., Laake, J.H., Ramírez-León, V., Roberg, B., Torgner, I., Kvamme, E., Usami, S., Ottersen, O.P., 1999. Phosphate activated glutaminase is concentrated in mitochondria of sensory hair cells in rat inner ear: a high resolution immunogold study. J. Neurocytol. 28 (3), 223–237.
Thalmann, R., Comegys, T.H., DeMott, J.E., Thalmann, I., 1981. Steep gradients of amino acids between cochlear endolymph and perilymph. Laryngoscope 91 (11), 1785–1791.
Thalmann, R., 1985. Gradients of organic substances between fluid compartments of the cochlea. Acta Otolaryngol. 99 (3–4), 469–477.
Usami, S., Osen, K.K., Zhang, N., Ottersen, O.P., 1992. Distribution of glutamate-like and glutamine-like immunoreactivities in the rat organ of Corti: a light microscopic and semiquantitative electron microscopic analysis with a note on the localization of aspartate. Exp. Brain Res. 91 (1), 1–11.
Varoqui, H., Zhu, H., Yao, D., Ming, H., Erickson, J.D., 2000. Cloning and functional identification of a neuronal glutamine transporter. J. Biol. Chem. 275 (5), 4049–4054.
Wiet, G.J., Godfrey, D.A., Ross, C.D., Dunn, J.D., 1986. Quantitative distributions of aspartate aminotransferase and glutaminase activities in the rat cochlea. Hear. Res. 24 (2), 137–150.

G Model
ANL-1699; No. of Pages 3

ARTICLE IN PRESS

Auris Nasus Larynx xxx (2012) xxx–xxx

Contents lists available at SciVerse ScienceDirect

Auris Nasus Larynx

journal homepage: www.elsevier.com/locate/anl

Cochlin-tomoprotein (CTP) detection test identified perilymph leakage preoperatively in revision stapes surgery

Yuko Kataoka [a,*], Tetsuo Ikezono [b], Kunihiro Fukushima [a], Koji Yuen [c], Yukihide Maeda [a], Akiko Sugaya [a], Kazunori Nishizaki [a]

[a] Department of Otorhinolaryngology, Head & Neck Surgery, Okayama University Postgraduate School of Medicine, Dentistry and Pharmaceutical Science, Japan
[b] Department of Otolaryngology, Saitama Medical University, Japan
[c] Yuen Clinic, Japan

ARTICLE INFO

Article history:
Received 14 March 2012
Accepted 14 September 2012
Available online xxx

Keywords:
Perilymphatic fistula
Stapes surgery
Cochlin
Cochlin-tomoprotein

ABSTRACT

Perilymphatic fistula (PLF) is defined as an abnormal leakage between perilymph from the labyrinth to the middle ear. Symptoms include hearing loss, tinnitus, and vertigo. The standard mode of PLF detection is intraoperative visualization of perilymph leakage and fistula, which ostensibly confirms the existence of PLF. Other possible methods of diagnosis include confirmation of pneumolabyrinth via diagnostic imaging. Recently, a cochlin-tomoprotein (CTP) detection test has been developed that allows definitive diagnosis of PLF-related hearing loss.

We report the case of a 45-year-old man who presented with right-sided tinnitus, hearing loss, and dizziness 30 years after stapes surgery. Middle ear lavage was performed after myringotomy. A preoperative diagnosis of PLF was reached using the CTP detection test. Intraoperative observations included a necrotic long process of the incus, displaced wire piston, and fibrous tissue in the oval window. Perilymph leakage was not evident. The oval window was closed with fascia, and vertigo disappeared within 2 weeks postoperatively. When PLF is suspected after stapes surgery, the CTP detection test can be a useful, highly sensitive, and less invasive method for preoperative diagnosis.

1. Introduction

Perilymphatic fistula (PLF) is defined as abnormal leakage between perilymph from the labyrinth to the middle ear. PLF diagnosis has been made with pneumolabyrinth in the inner ear on computed tomography (CT) and T2-weighted magnetic resonance imaging (MRI) [1]. Leakage has been confirmed during open and endoscopic surgery [2,3]. However, PLF diagnosis is clinically difficult because CT, MRI, and perioperative methods are not always able to detect the leakage.

In 2001, cochlin-tomoprotein (CTP), a novel perilymph-specific protein, was identified [4]. CTP is a protein product of *COCH*, which was originally identified from the cochlea-specific cDNA library. Later, its mutation was found to be associated with DFNA9, an autosomal dominant hereditary deafness condition. Three cochlin isoforms were identified; CTP was one of these short 16-kDa isoforms. CTP is found in the functional domain of LCCL in cochlin and is secreted to the perilymph. CTP is highly specific for perilymph. Therefore, a diagnosis of PLF can be made by detection of CTP using Western blotting in lavage of the middle ear [5].

We report a case of right-sided tinnitus, hearing loss, and dizziness manifesting 30 years after stapes surgery. PLF was diagnosed preoperatively using the CTP test in middle ear washings. PLF was not suspected based on clinical manifestations, eardrum examination, and CT. Preoperative diagnosis was possible only because of the CTP test. CTP detection test is a new, highly sensitive, less invasive, and useful method to aid in the diagnosis of PLF.

2. Case report

The patient was a 45-year-old man. In 1980, right stapes surgery had been performed on him and a Teflon wire piston was placed (details of the surgery were uncertain). The patient presented at our hospital with right-sided tinnitus of idiopathic origin. In December 2009, he experienced mild dizziness, but no rotatory vertigo or awareness of hearing loss was evident. In an audiometric test, deterioration of hearing by bone conduction was detected as compared with hearing level recorded during a consultation conducted 20 years previously. Therefore acute mixed hearing loss was suspected.

* Corresponding author at: Department of Otorhinolaryngology, Head & Neck Surgery, Okayama University Postgraduate School of Medicine, Dentistry and Pharmaceutical Science, 2-5-1 Shikata-cho, Kita-ku, Okayama City, Okayama 700-8558, Japan. Tel.: +81 86 235 7307; fax: +81 86 235 7308.
E-mail address: yu-kat@cc.okayama-u.ac.jp (Y. Kataoka).

0385-8146/$ – see front matter © 2012 Published by Elsevier Ireland Ltd.
http://dx.doi.org/10.1016/j.anl.2012.08.001

Please cite this article in press as: Kataoka Y, et al. Cochlin-tomoprotein (CTP) detection test identified perilymph leakage preoperatively in revision stapes surgery. Auris Nasus Larynx (2012), http://dx.doi.org/10.1016/j.anl.2012.08.001

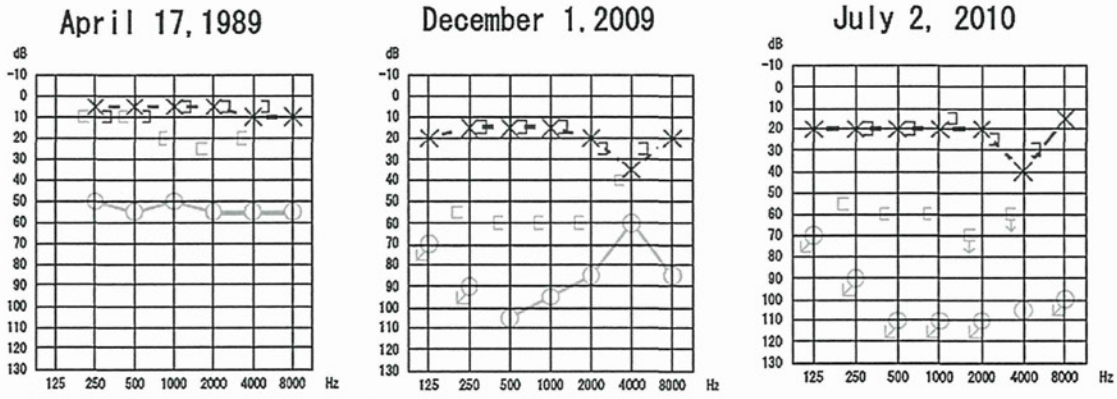

Fig. 1. Audiogram. Hearing levels in December 2009 where lower than those in 1989. In July 2010, vertigo developed, and hearing deteriorated further.

Administration of oral prednisolone (30 mg per day), ATP, and vitamin B12 was initiated. At the end of June 2010, rotatory vertigo and tinnitus appeared and hearing in the right ear deteriorated further (Fig. 1). Pure horizontal nystagmus directed to the left was observed under Frenzel glasses. On physical examination, no fluid was found in the tympanic cavity through the right tympanic membrane.

Hydrocortisone sodium succinate was administered via intravenous drip (500 mg per day) for 10 days tapering starting on July 2, 2010. Rotatory vertigo was gradually relieved, but dizziness continued. On the basis of clinical history, PLF was suspected. We obtained informed consent from him and collected middle ear washings after myringotomy under topical anesthesia and examined by the CTP detection test. The procedure of this test has been reported previously [4]. A CTP-positive signal was observed from the middle ear washings (Fig. 2), confirming the diagnosis of right PLF. After and during the test, no exacerbation of dizziness, tinnitus, or hearing loss was observed.

On November 1, 2010, surgery was performed under general anesthesia. Intraoperative observations included a necrotic long process of the incus, displaced wire piston, and fibrous tissue in the oval window. The body and short process of the incus were in the normal position. The incus and wire were transected and the wire of the piston was visible outside the oval window, but the piston was found lying deep within the vestibule. The footplate of the stapes was not found. Leakage of lymph fluid into the tympanic cavity and around the oval and round windows was not observed. Fibrous adhesions, mucosal hyperplasia, and the wire piston were removed.

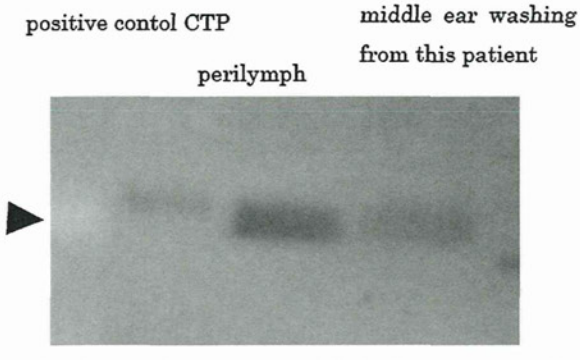

Fig. 2. Detection of cochlin-tomoprotein (CTP) in the middle ear washings. Signals represent CTP in recombinant positive control CTP (left), perilymph (middle), and middle ear washings from the patient (right) by Western blotting.

The oval and round windows were covered with the temporal fascia using fibrin glue to seal the fistula, but no prosthesis was used for the purpose of hearing improvement.

Postoperatively, mild dizziness was observed, but rotatory vertigo and nystagmus disappeared. The dizziness gradually improved and the patient was discharged 12 days after surgery.

3. Discussion

PLF causes inner ear disorders due to perilymph leakage into the tympanic cavity. PLF can be associated with a congenital anomaly, postoperative ear complications, head trauma, or barotrauma, but is most often idiopathic. PLF presents with symptoms of hearing loss, tinnitus, vestibular vertigo or dizziness, popping sounds, streaming tinnitus, and fistula signs. However, it is often indistinguishable from other inner ear diseases.

In some cases of PLF, pneumolabyrinth (air in the inner ear) and liquid leakage into the tympanic cavity can be detected by high-resolution temporal bone CT or T2-weighted MRI [1]. Although the gold standard for PLF diagnosis is intraoperative microscopic or endoscopic visualization, PLF is difficult to identify even during surgery [2,3]. Bakhos et al. [6] and Vincent et al. [7] reported that perilymphatic leakages were identified in 8% and 5.5%, respectively, of cases of revision stapes surgery. Furthermore, in their studies, PLF was suspected preoperatively in 36 cases based on clinical symptoms, but fistula was observed only in 23 cases and in 13 of them, fistula was not diagnosed due to perioperative findings [7].

Proteomic analysis of inner ear proteins identified the unique properties of CTP [4]. CTP is a protein present in perilymph, but not in other body fluids such as cerebrospinal fluid (CSF), serum, saliva, or middle ear mucosa. Therefore, CTP may be considered a specific biochemical marker for perilymph [5].

The sensitivity of the CTP test is 92.3% from middle ear lavage fluid sampled after cochlear fenestration in cochlear implant surgery [8]. While its specificity is 98.2% from middle ear lavage of non-PLF cases without middle ear infections [9]. Analysis of middle ear lavage fluid sampled from patients with middle ear infections may provide false-positive results (e.g., specificity of 93.5%) because of the high protein concentration in the thick pus [9]. In this study, CTP was detected in approximately 1 μl of perilymph present in the middle ear cavity. This method may enable diagnosis of PLF from minimal amounts of leaked perilymph, which is difficult to detect by CT and MRI or perioperatively. This method is also less invasive, as lavage can be performed by myringotomy or puncture of the tympanic membrane.

Several authors have suggested identification of an endogenous perilymph marker such as beta-2 transferrin, beta trace protein, or

Please cite this article in press as: Kataoka Y, et al. Cochlin-tomoprotein (CTP) detection test identified perilymph leakage preoperatively in revision stapes surgery. Auris Nasus Larynx (2012), http://dx.doi.org/10.1016/j.anl.2012.08.001

intrathecal fluorescein [10–12]. Although these markers are also detectable in inner ear fluid, PLF and CSF leakage can be difficult to distinguish because they are not organ specific.

In our case, the wire piston had transferred deep into the vestibule behind the long limb of the incus necrosis. Perilymph leakage occurred, leading to rotatory vertigo and deterioration of hearing. PLF was not initially suspected because 30 years had passed since stapes surgery, and typical symptoms of PLF were not present. In addition, effusion in the tympanic cavity was not detected on examination of the tympanic membrane. Thus, diagnosis of PLF was impossible by visual inspection alone or imaging techniques such as CT and MRI. The CTP detection test was the only method for detecting perilymph leakage in this case.

Our experience suggests that the CTP detection test can be a useful, highly sensitive, specific, and less invasive method to diagnose local manifestations of PLF.

Conflict of interest

The authors report no conflicts of interest.

Acknowledgements

This work was partly supported by a grant from the Ministry of Health, Labor, and Welfare, Japan and the Ministry of Education, Culture, Sports, Science, and Technology, Japan. The authors would like to thank Enago (http://www.enago.jp) for the English language review.

References

[1] Nishizaki K, Yamamoto T, Akagi H, Ogawa T, Masuda Y. Imaging case of the month. Pneumolabyrinth. Am J Otol 1998;19:860–1.
[2] Ogawa K, Kanzaki J, Ogawa S, Tsuchihashi N, Inoue Y, Yamamoto M. Endoscopic diagnosis of idiopathic perilymphatic fistula. Acta Otolaryngol Suppl 1994;514:63–5.
[3] Poe DS, Rebeiz EE, Pankratov MM. Evaluation of perilymphatic fistulas by middle ear endoscopy. Am J Otol 1992;13:529–33.
[4] Ikezono T, Shindo S, Li L, Omori A, Ichinose S, Watanabe A, et al. Identification of a novel Cochlin isoform in the perilymph: insights to Cochlin function and the pathogenesis of DFNA9. Biochem Biophys Res Commun 2004;314:440–6.
[5] Ikezono T, Shindo S, Sekiguchi S, Hanprasertpong C, Li L, Pawankar R, et al. Cochlin-tomoprotein: a novel perilymph-specific protein and a potential marker for the diagnosis of perilymphatic fistula. Audiol Neurootol 2009;14:338–44.
[6] Bakhos D, Lescanne E, Charretier C, Robier A. A review of 89 revision stapes surgeries for otosclerosis. Eur Ann Otorhinolaryngol Head Neck Dis 2010;127:177–82.
[7] Vincent R, Rovers M, Zingade N, Oates J, Sperling N, Devèze A, et al. Revision stapedotomy: operative findings and hearing results. A prospective study of 652 cases from the Otology–Neurotology Database. Otol Neurotol 2010;31:875–82.
[8] Ikezono T, Sugizaki K, Shindo S, Sekiguchi S, Pawankar R, Baba S, et al. CTP (cochlin-tomoprotein) detection in the profuse fluid leakage (gusher) from cochleostomy. Acta Otolaryngol 2010;130:881–7.
[9] Ikezono T, Shindo S, Sekiguchi S, Morizane T, Pawankar R, Watanabe A, et al. The performance of cochlin-tomoprotein detection test for the diagnosis of perilymphatic fistula. Audiol Neurootol 2009;15:168–74.
[10] Buchman CA, Luxford WM, Hirsch BE, Fucci MJ, Kelly RH. Beta-2 transferrin assay in the identification of perilymph. Am J Otol 1999;20:174–8.
[11] Bachmann-Harildstad G, Stenklev NC, Myrvoll E, Jablonski G, Klingenberg O. β-Trace protein as a diagnostic marker for perilymphatic fluid fistula: a prospective controlled pilot study to test a sample collection technique. Otol Neurotol 2011;32:7–10.
[12] Gehrking E, Wisst F, Remmert S, Sommer K. Intraoperative assessment of perilymphatic fistulas with intrathecal administration of fluorescein. Laryngoscope 2002;112:1614–8.

Please cite this article in press as: Kataoka Y, et al. Cochlin-tomoprotein (CTP) detection test identified perilymph leakage preoperatively in revision stapes surgery. Auris Nasus Larynx (2012), http://dx.doi.org/10.1016/j.anl.2012.08.001

Acta Oto-Laryngologica, 2012; 132: 1134–1139

informa
healthcare

ORIGINAL ARTICLE

Cochlin expression in the rat perilymph during postnatal development

KYOKO SHIIBA[1], SUSUMU SHINDO[2], TETSUO IKEZONO[2], KUWON SEKINE[1], TOMOHIRO MATSUMURA[3], SATOMI SEKIGUCHI[4], TOSHIAKI YAGI[5] & KIMIHIRO OKUBO[1]

[1]*Department of Otorhinolaryngology, Nippon Medical School, Tokyo,* [2]*Department of Otorhinolaryngology, Saitama Medical University Faculty of Medicine, Iruma, Saitama,* [3]*Department of Biochemistry and Molecular Biology, Nippon Medical School, Tokyo,* [4]*R&D and Business Development Segment, Mitsubishi Chemical Medience Corporation, Tokyo and* [5]*University of Human Environments, Okazaki, Aichi, Japan*

Abstract

Conclusions: The changes in the cochlin isoforms in the perilymph may provide important insights to the understanding of cochlin function and the pathogenesis of related inner ear diseases. *Objectives*: Cochlin is involved in various pathologies of the inner ear. Altered levels of cochlin isoforms in developing inner ear tissue were reported previously. The purpose of this study was to elucidate the cochlin isoform expression in the perilymph of rats during postnatal development in relation to Coch gene mRNA expression. *Methods*: We studied the cochlin isoforms in the rat perilymph during postnatal development by Western blot analysis. Real-time PCR was also performed to elucidate the expression level of Coch mRNA in the developing inner ear of rats. *Results*: Western blot analysis showed that the expression of p63s in the perilymph was highest on the 12th day after birth (DAB12), the earliest age at which we could identify the perilymphatic space microscopically, and it decreased gradually as the cochlea developed. On the other hand, the expression of Cochlin-tomoprotein (CTP)was lowest on DAB12 and increased gradually up to DAB24. COCH mRNA was detected from DAB3 and gradually increased to DAB15, and then gradually decreased to DAB70.

Keywords: *DFNA9, COCH gene, Western blot, real-time PCR*

Introduction

The COCH (coagulation factor C homology) gene, which encodes the abundant inner ear protein cochlin, has been shown to be mutated in the autosomal dominant, late-onset, and progressive nonsyndromic hearing loss and vestibular disorder DFNA9. To date, 13 different missense mutations and one in-frame deletion have been reported in patients [1–4]. Balance problems, vertigo, positional nystagmus, dizziness, tinnitus, night blindness, memory loss, and cardiovascular diseases have been reported in the affected family members [5,6]. Cochlin is also a prominent target antigen in CD4+ T-cell-mediated autoimmune hearing loss [7]. Additionally, increased levels of cochlin have been found in the trabecular meshwork of glaucomatous mice and are presumed to have a causal role in the development of increased intraocular pressure and glaucoma [8]. Cochlin is thus clearly involved in various pathologies of the inner ear and eye. However, the precise mechanisms underlying the pathogenesis and the function of the cochlin protein, the most highly expressed protein in the human and mouse inner ear, at present still remain unclear.

We have conducted a series of studies to elucidate the cochlin isoforms and the mechanism of expression. The three cochlin isoforms p63s, p44s, and p40s, were detected in the inner ear tissue and a short 16 kDa isoform, Cochlin-tomoprotein (CTP), was

Correspondence: Tetsuo Ikezono MD PhD, Department of Otorhinolaryngology, Saitama Medical University Faculty of Medicine, Iruma, Saitama 350-0495, Japan. Tel: +81 49 276 1253. Fax: +81 49 295 8061. E-mail: ikez@saitama-med.ac.jp

(Received 26 February 2012; accepted 14 April 2012)

ISSN 0001-6489 print/ISSN 1651-2251 online
DOI: 10.3109/00016489.2012.687456

found in the perilymph [9,10]. We also show that dynamic changes occur in cochlin isoform expression during postnatal development in the rat inner ear. Both immunohistochemistry and Western blot analysis showed an increase in the expression of the total amount of cochlins [11] during development. The level of expression of p63s was the highest among the three isoforms between the 17th day after birth (DAB17) and DAB24. In contrast, on DAB70, the expression of p63s had decreased and p40s had become the predominant isoform. The importance of isoform analysis was reported in a study of Usher syndrome type 1F (USH1F) [12], where altered levels of cochlin isoforms were suggested to be pathogenic.

To determine how expressions of COCH isoforms are controlled, we investigated the perilymph in this study. Contrary to expectations, Western blot analysis showed that the expression of p63s in the perilymph was the highest on DAB12, the earliest age at which the perilymphatic space could be visualized microscopically, and decreased gradually as the cochlea developed. On the other hand, the expression of CTP was lowest on DAB12 and increased gradually to DAB24. Coch mRNA was detected on DAB3. This study demonstrates the temporal changes in the expression of the cochlin isoforms in the perilymph of the developing ear of the rat.

Material and methods

Animals

For real-time PCR, the inner ear membranous labyrinth was excised from Wistar rats (Sankyo Labo Service Corporation, Tokyo, Japan) including the temporal bones on DAB3 and DAB6 (n = 20 ears for each group), as well as DAB 9, 12, 15, 24, 36, and 70 (n = 10 ears for each group), and the samples were mixed in each group. The perilymph was collected as follows. Under microscopy, after removing the stapes, the perilymphatic space was identified and the perilymph was suctioned out slowly with a thin pipette, taking special care not to touch or damage the membranous labyrinth. In the preliminary stage of the experiment, we investigated the identification of the perilymphatic space, and DAB12 was the youngest age at which perilymph could be collected. Wistar rats on DAB12 and 18 (n = 8 ears for each group) as well as DAB 24, 30, and 70 (n = 4 ears for each group) were used for Western blot analysis of the perilymph and the samples were mixed for each group.

For the performance of the experimental procedure, each rat was deeply anesthetized with sodium pentobarbital (50 mg/kg, i.p.) This study was approved by the Animal Experimentation Ethics Committee (No. 19-108, approved on May 16, 2008) of Nippon Medical School.

Western blot

Since human, bovine, and rat perilymph contains two cochlin isoforms, the full-length isoform p63 and the short truncated isoform CTP, we used the rabbit polyclonal anti-LCCL-C Ab (Figure 1), which recognizes these isoforms [10,13]. This antibody was prepared as described previously [10]. In brief, a 14-mer peptide (LSRWSASFTVTKGK) corresponding to residues 114–127 of the LCCL (Limulus factor C, Coch-5b2, and Lgl1) domain was used to generate the antibody. We added cysteine residues to the C termini of the peptides to permit coupling of the peptides to KLH as a carrier protein for immunization. Rabbits were immunized by repeated subcutaneous injections of the KLH-coupled peptides. The serum was purified using a protein A column, followed by peptide-affinity chromatography. The specificity of the antibodies for the corresponding antigenic peptides was confirmed by dot-blot analysis and a peptide absorption test (data not shown).

The perilymph was centrifuged at 1000 g for 15 min and the supernatant was stored at –80°C until use. Then 0.5 µl of each perilymph sample was loaded onto a 15% SDS-polyacrylamide gel. Before loading, samples were diluted with 0.188 M Tris buffer to a total volume of 10 µl and mixed with 5 µl of sample buffer (0.188 M Tris buffer, 2.39 mM SDS, 30% glycerol, and 15% 2-mercaptoethanol). The samples

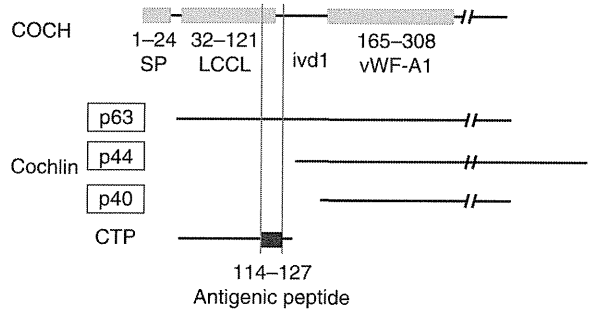

Figure 1. Representation of the antigenic peptide location, and the COCH gene, cochlin, and CTP. The top line denotes the deduced amino acid sequence of human COCH, showing the positions of the signal peptide (SP), Limulus factor C, cochlin, the late gestation lung protein Lgl1 domain (LCCL), intervening domain 1 (ivd1), and von Willebrand factor type A-like domain 1 (vWF-A1). The middle lines depict the cochlin isoforms p63s, p44s, and p40s that are expressed in inner ear tissue. The bottom line depicts the cochlin-tomoprotein (CTP) isoform expressed in the perilymph. The black bar indicates the location of the antigenic peptide and vertical lines represent the alignment of the antigenic peptide and cochlin isoforms. The numbers indicate the corresponding amino acid sequence of human cochlin.

were heated to 98°C for 5 min and then loaded into each lane of the gel. Electrophoresis was performed on 15% polyacrylamide gels (PAG mini Daiichi, Daiichi Pure Chemicals, Japan) in running buffer (25 mM Tris, 192 mM glycine, 1 g/l SDS, pH 8.3) at 20 mA for 2 h. The separated proteins were electrophoretically transferred onto a PVDF membrane (Immobilon-PSQ, Millipore, USA) using an Atto HorizBlot semi-dry transfer unit with a discontinuous buffer system, as recommended by the manufacturer (ATTO, Japan). Nonspecific binding was blocked by incubating the membranes overnight at 4°C in 5% skimmed milk and 0.2% polyoxyethylene sorbitan (Tween-20) dissolved in PBS. Membranes were then incubated in PBS containing 1% skimmed milk and 0.1% Tween-20 for 2 h at room temperature with the primary anti-LCCL-C Ab diluted at 1:2000. After washing in 0.05% Tween-20 in PBS, membranes were incubated for 1 h at room temperature with horseradish peroxidase-labeled goat anti-rabbit IgG (P0448, Dako, Denmark) diluted at 1:5000 in the same buffer used for the primary antibody reaction. The membranes were washed again and the reaction was developed with a chemiluminescence reaction kit (ECL Advance, GE Healthcare, England). The protein expression level of each isoform was determined with a densitometer LAS-3000 (Fuji Film, Japan), and the relative amount in each lane was calculated based on the p63 signal on DAB12 and the CTP signal on DAB24, respectively.

Real-time PCR

RNA preparation. Inner ear tissue was stored in RNAlater reagent (QIAGEN Inc., Mississauga, ON, Canada) at –80°C until RNA extraction. For the extraction of RNA, tissue was homogenized using 1.5 ml pellet pestles with Matching Microtubes (Kimble-Kontes, Vineland, NJ, USA) and QIAshredder spin columns (QIAGEN). Total RNA was extracted using an Ambion mirVana™ miRNA Isolation Kit (Applied Biosystems, Foster City, CA, USA) following the manufacturer's protocol. The RNA concentration was determined by measuring absorbance at 260 nm with a spectrophotometer UV-1800 (Shimadzu, Kyoto, Japan), and the RNA concentration was normalized to 50 ng/μl.

Reverse transcription. Total RNAs from the membranous labyrinth were reverse-transcribed using a TaKaRa PCR Kit (AMV) Ver3.0 (Takara bio, Ohtsu, Shiga, Japan) with an oligo-dT-adapter primer for 30 min at 50°C, 5 min at 95°C, and 5 min at 5°C using a thermal cycler GeneAmp® PCR System 9700 (Applied Biosystems).

Real-time PCR assay validation. We conducted a preliminary study to validate the detection method, and verified the amplification efficiencies of COCH and the housekeeping gene GAPDH (glyceraldehyde-3-phosphate dehydrogenase) using RNA from the rat inner ear. The differences in the threshold cycle (ΔC_T) between COCH and GAPDH at serial dilutions of cDNA samples (×4, ×20, ×100, and ×500) were evaluated.

Real-time PCR assay. All the real-time PCR samples were set up in Fast96Well optical plates using 1 μl of cDNA. The reaction mixture was prepared using COCH primers (TaqMan Gene Expression Assays: Assay ID; Hs00187937_m1 Gene Symbol; hCG40905 Applied Biosystems). Since no TaqMan Gene Expression Assay targeting N terminus COCH mRNA was available, we selected a probe covering exon 8–9, which encodes the N-terminal portion of p40. Then 10 μl of 2× TaqManUniversal PCR Master Mix 10, 1 μl of 20× Primer&Probe Mixture, and 8 μl of RNA-free water were added to a final volume of 20 μl per reaction. GAPDH was used as a housekeeping gene. Then 10 μl of 2× TaqManUniversal PCR Master Mix (Applied Biosystems), 0.9 μl of 10 μM Forward and Reverse Primers, 0.5 μl of 5 μM TaqManProbe, and 6.7 μl of RNA-free water were added to a final volume of 20 μl per reaction.

All the samples were tested in triplicate. The real-time PCR program consisted of incubation at 50°C for 2 min, and 95°C for 10 min, 40 cycles at 95°C for 15 s, and 60°C for 1 min using the 7500 Real-Time PCR System (Applied Biosystems).

Data were evaluated using the $\Delta\Delta C_T$ method [14,15]. The method of Livak and Schmittgen [15] and the reference ΔC_T values obtained from the biological control GAPDH were applied for calculation of $\Delta\Delta C_T$ and the relative quantity values, respectively.

Results

Western blot analysis of cochlin isoform expression in the rat perilymph

The perilymph samples of eight ears (DAB12 and 18) and four ears (DAB 24, 30, and 70) were mixed and 0.5 μl of each sample was loaded into one lane. Using anti-LCCL-C Ab, immunoreactive proteins of 63 kDa and 16 kDa (CTP) were detected (Figure 2A). The level of protein expression for each was measured with a densitometer (LAS-3000; Fuji Film, Japan), and the relative amount of each band was calculated relative to the expression of p63 on DAB12, with the CTP on DAB18 taken as 100. Analysis was performed in triplicate and the data are presented as the mean ± standard

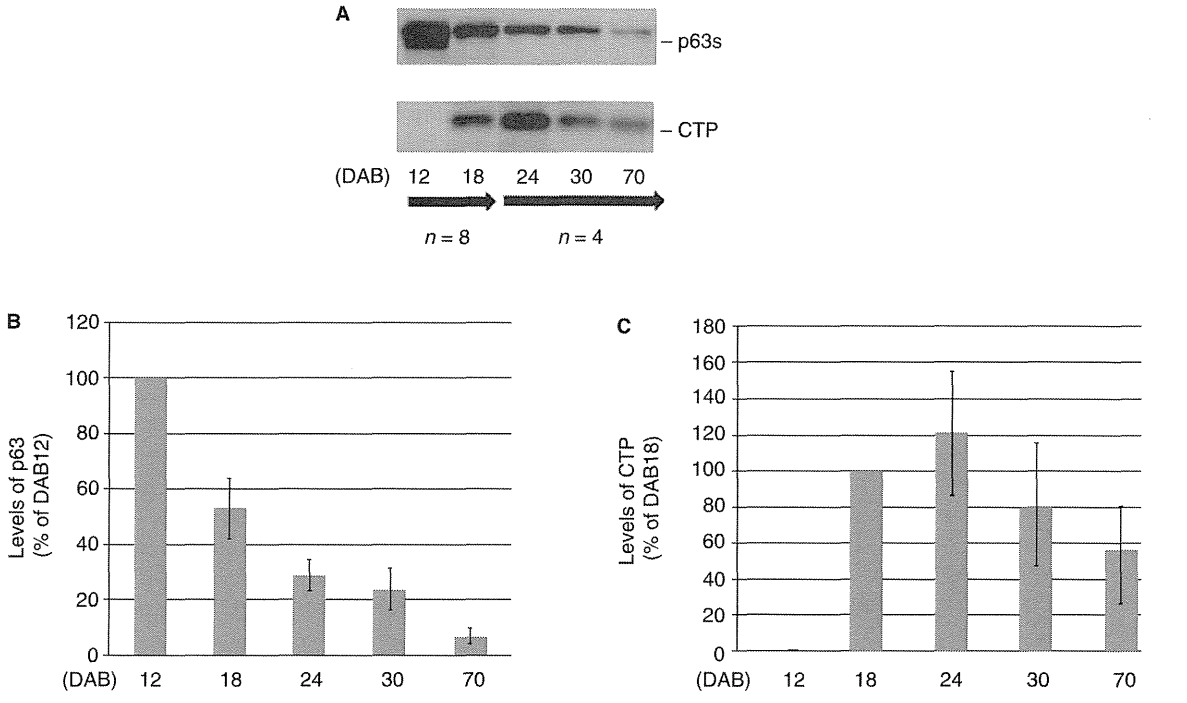

Figure 2. (A) Western blot analysis of perilymph proteins from the rat. Wistar rats on DAB 12 and 18 (n = 8 ears for each group) as well as DAB, 24, 30, and 70 (n = 4 ears for each group) were used for Western blot analysis of the perilymph. The samples from these ears were mixed for each DAB group. A representative Western blot is shown. The anti-LCCL-C antibody detected immunoreactive proteins of 63 kDa and 16 kDa (cochlin-tomoprotein, CTP). (B and C) The protein expression level of each of the isoforms in the perilymph: p63 (B) and CTP (C). The protein expression level of each isoform in the perilymph was measured by an LAS-3000 densitometer (Fuji Film, Japan), and the relative amount of each isoform was calculated relative to the expression of p63 on DAB12, with CTP on DAB18 taken as 100. Analysis was performed in triplicate and the data are presented as the mean ± standard error.

error. On DAB12, p63 expression was the highest among the perilymph samples tested and it gradually decreased to 52.8 ± 10.9% by DAB18, 28.7 ± 5.5% on DAB24, 23.7 ± 7.3% on DAB30, and then 6.7 ± 2.9% on DAB70. On the other hand, CTP expression was not detected on DAB12, detected on DAB18, and reached a peak of 121.4 ± 33.6% on DAB24. Then it gradually subsided to 80.3 ± 35.3% on DAB 30 and 56.7 ± 24.2% on DAB 70 (Figure 2B, C).

Real-time PCR assay validation

The threshold cycle (ΔC_T) difference between COCH and GAPDH in a serial dilution of cDNA samples (×4, ×20, ×100, and ×500) gave a linear slope of 0.0185, indicating that these genes have proportional expression efficiencies (Figure 3). It was appropriate to use the $\Delta\Delta C_T$ method since the slope of the standard curves of the COCH was <0.1.

Real-time PCR assay

The inner ear tissue of 20 ears (DAB 3, 6) or 10 ears (DAB 9, 12, 15, 24, 36, 70) was mixed and analyzed using real-time PCR assay. Comparative C_T ($\Delta\Delta C_T$) analysis was performed to evaluate the fold changes in mRNA expression. Analysis was performed in triplicate and the data are presented as the mean ± standard error. As shown in Figure 4, COCH mRNA was detected on DAB3, and continued to increase, reaching a maximum of 56.36 ± 0.84-fold on DAB15. Then it began to decrease gradually, and it was 10.73 ± 2.83-fold on DAB70.

Discussion

Cochlin, which is encoded by *COCH*, is a secreted protein for which the function is not completely understood, but it is believed to have a role in the formation and/or maintenance of the extracellular matrix (ECM) in the inner ear [1,16]. Cochlin appears to have numerous heterogeneous isoforms that are caused partly by N-glycosylation and proteolytic cleavage, and potentially also by alternative splicing [9,10,13,17]. Previous 2D gel investigation identified a full-length isoform, as well as smaller isoforms with truncations of the N terminus. The molecular weight values of the predominant isoforms were 44 and 40 kDa [10,12].

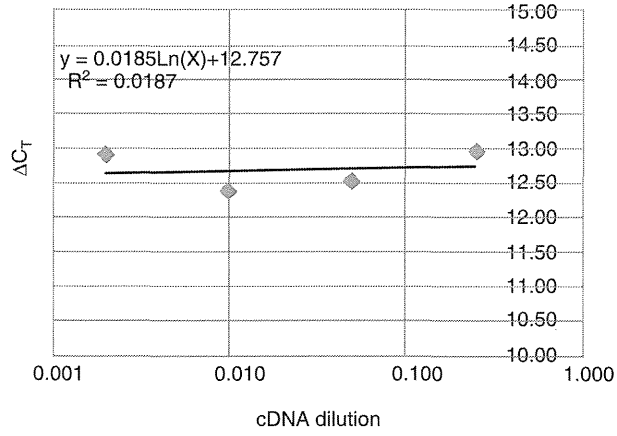

Figure 3. Real-time PCR assay validation. The differences in threshold cycle (ΔC_T) between COCH and GAPDH at serial dilution of cDNA samples (×4, ×20, ×100, and ×500) gave a lineal slope of 0.0185, indicating that both genes have proportional expression efficiencies.

Isoform-specific antibodies further identified the short truncated isoform CTP in the perilymph [10], and this isoform contains the N-terminal LCCL domain devoid of the C-terminal vWFA domain. The molecular weight of CTP is different in different species, e.g. rat (11–17 kDa), human (16 kDa), and bovine (18–23 kDa) [13].

The importance of cochlin has been shown in a variety of pathological conditions, such as DFNA9, autoimmune hearing loss, glaucoma, and others. One of the keys to understanding the pathogenetic mechanisms in these conditions is the analysis of the isoform expression patterns. Chance et al. [12] identified certain proteins and protein networks associated with cochlear pathogenesis in the Ames Waltzer (*av*)

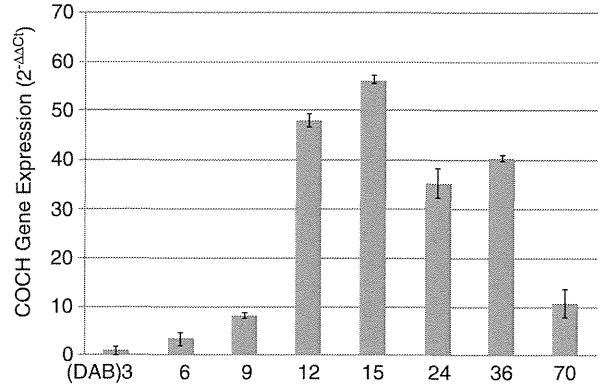

Figure 4. Real-time PCR assay of COCH gene expression in the developing inner ear tissue. The inner ear tissue of 20 ears (DAB 3, 6) or 10 ears (DAB 9, 12, 15, 24, 36, 70) was mixed and analyzed using real-time PCR assay. Comparative C_T ($\Delta\Delta C_T$) analysis was performed to evaluate the fold changes in mRNA expression. Analysis was performed in triplicate and the data are presented as the mean ± standard error.

mouse, a model for deafness in Usher syndrome 1F (USH1F). Sequence analysis by mass spectrometry showed that, in the *av* cochlea, a set of full-length cochlin isoforms was up-regulated, while the isoforms lacking the N-terminal FCH/LCCL domain were down-regulated. The potential effects that are conveyed by this molecular phenotype are currently unknown, but the observed change is counter to what has been reported in normal development. Our previous data indicated that the abundance of the full-length isoform p63s decreases relative to the abundance of the N-terminally truncated form p44s and p40s as a function of age in the rat, with the full-length isoform predominant on DAB24 but decreased relative to the truncated form on DAB70 [11,12].

In the present study, contrary to expectations, Western blot analysis showed that the expression of p63s in the perilymph was the highest on DAB12 and decreased gradually as the cochlea developed. On the other hand, CTP expression was lowest on DAB12 and increased gradually to DAB24. In our previous study of cochlin isoform expression analysis in inner ear tissue [11], p63s was below the detection limit on DAB13, but its expression gradually increased up to DAB24. On DAB70, p63s expression was lower than on DAB24. The N-terminally truncated forms, p44s and P40s, were not detected at DAB13 and were only weakly expressed from DAB17 to DAB70, although the expression did gradually increase up to DAB70 [11]. Notably, this change in p63 expression in the inner ear tissue is counter to what was found in the perilymph. p63 may be secreted into the perilymph in the early stage of postnatal inner ear development and then gradually come to be expressed in the inner ear tissue. The real-time PCR data on COCH expression confirmed the gene expression in the early stages, even though the expression level was minimal compared with that of DAB 12–24. The dynamic changes in the expression of the cochlin isoforms in the postnatal inner ear development suggest that cochlin plays an important role in the development and maturation process of the inner ear.

Perilymph is an important fluid not only for the delivery of the mechanical vibrations to hair cells, but also in the homeostatic regulation of certain ionic components, proteins, and other molecules, and it also provides a crucial microenvironment for labyrinthine cells. In our preliminary investigation, it was possible to microscopically identify the perilymphatic space as early as DAB12, and perilymph by itself could be collected without any other tissue contamination. Human, bovine, and rat perilymph contain two cochlin isoforms, the full-length isoform p63 and the short truncated isoform CTP [10,13]. The origin of these cochlin isoforms has been attributed to a variety of mechanisms, including proteolysis of

peptide bonds, chemical modifications such as glycosylation, phosphorylation and/or deamination, and multiple transcripts [9,17–19]. CTP may be formed by post-translational cleavage from full-length cochlin or directly encoded by a unique COCH gene splice variant [13]. Of the 13 DFNA9 mutations now reported for the COCH gene, 10 affect the residues of the LCCL domain. Yao et al. recently showed that full-length cochlin with mutations in this domain is cytotoxic when it is introduced into the perilymphatic space in vivo [20]. This study also suggests that mutant CTP in the perilymph may be harmful to inner ear function.

An adequate elucidation of the formation and processing of the cochlin isoforms, including the isoforms expressed in the perilymph, would provide insight into cochlin in the developing ear and mechanistic clues to how it is that mutations in the COCH gene damage the inner ear and other organs.

Declaration of interest: The authors report no conflicts of interest. The authors alone are responsible for the content and writing of the paper.

References

[1] Robertson NG, Lu L, Heller S, Merchant SN, Eavey RD, McKenna M, et al. Mutations in a novel cochlear gene cause DFNA9, a human nonsyndromic sensorineural deafness with vestibular dysfunction. Nat Genet 1998;20:299–303.

[2] de Kok YJ, Bom SJ, Brunt TM, Kemperman MH, van Beusekom E, van der Velde-Visser SD, et al. A Pro51Ser mutation in the COCH gene is associated with late onset autosomal dominant progressive sensorineural hearing loss with vestibular defects. Hum Mol Genet 1999;8:361–6.

[3] Usami S, Takahashi K, Yuge I, Ohtsuka A, Namba A, Abe S, et al. Mutations in the *COCH* gene are a frequent cause of autosomal dominant progressive cochleo-vestibular dysfunction, but not of Meniere's disease. Eur J Hum Genet 2003;11:744–8.

[4] Jones SM, Robertson NG, Given S, Giersch AB, Liberman MC, Morton CC. Hearing and vestibular deficits in the Coch(-/-) null mouse model: comparison to the Coch (G88E/G88E) mouse and to DFNA9 hearing and balance disorder. Hear Res 2011;272:42–8.

[5] Hildebrand MS, Gandolfo L, Shearer AE, Webster JA, Jensen M, Kimberling WJ, et al. A novel mutation in COCH – implications for genotype-phenotype correlations in DFNA9 hearing loss. Laryngoscope 2010;120:2489–93.

[6] Bom SJ, Kemperman MH, De Kok YJ, Huygen PL, Verhagen WI, Cremers FP, et al. Progressive cochleovestibular impairment caused by a point mutation in the COCH gene at DFNA9. Laryngoscope 1999;109:1525–30.

[7] Baek MJ, Park HM, Johnson JM, Altuntas CZ, Jane-Wit D, Jaini R, et al. Increased frequencies of cochlin-specific T cells in patients with autoimmune sensorineural hearing loss. J Immunol 2006;177:4203–10.

[8] Bhattacharya SK, Rockwood EJ, Smith SD, Bonilha VL, Crabb JS, Kuchtey RW, et al. Proteomics reveal Cochlin deposits associated with glaucomatous trabecular meshwork. J Biol Chem 2005;280:6080–4.

[9] Ikezono T, Omori A, Ichinose S, Pawankar R, Watanabe A, Yagi T. Identification of the protein product of the Coch gene (hereditary deafness gene) as the major component of bovine inner ear protein. Biochim Biophys Acta 2001;1535: 258–65.

[10] Ikezono T, Shindo S, Li L, Omori A, Ichinose S, Watanabe A, et al. Identification of a novel Cochlin isoform in the perilymph: insights to Cochlin function and the pathogenesis of DFNA9. Biochem Biophys Res Commun 2004; 314:440–6.

[11] Shindo S, Ikezono T, Ishizaki M, Sekiguchi S, Mizuta K, Li L, et al. Spatiotemporal expression of cochlin in the inner ear of rats during postnatal development. Neurosci Lett 2008;444:148–52.

[12] Chance MR, Chang J, Liu S, Gokulrangan G, Chen DH, Lindsay A, et al. Proteomics, bioinformatics and targeted gene expression analysis reveals up-regulation of cochlin and identifies other potential biomarkers in the mouse model for deafness in Usher syndrome type 1F. Hum Mol Genet 2010; 19:1515–27.

[13] Sekine K, Ikezono T, Matsumura T, Shindo S, Watanabe A, Li L, et al. Expression of cochlin mRNA splice variants in the inner ear. Audiol Neurootol 2010;15:88–96.

[14] Schmittgen TD, Livak KJ. Analyzing real-time PCR data by the comparative C(T) method. Nat Protoc 2008;3: 1101–8.

[15] Livak KJ, Schmittgen TD. Analysis of relative gene expression data using real-time quantitative PCR and the 2(-Delta Delta C(T)) Method. Methods 2001;25:402–8.

[16] Robertson NG, Cremers CW, Huygen PL, Ikezono T, Krastins B, Kremer H, et al. Cochlin immunostaining of inner ear pathologic deposits and proteomic analysis in DFNA9 deafness and vestibular dysfunction. Hum Mol Genet 2006;15:1071–85.

[17] Kommareddi PK, Nair TS, Raphael Y, Telian SA, Kim AH, Arts HA, et al. Cochlin isoforms and their interaction with CTL2 (SLC44A2) in the inner ear. J Assoc Res Otolaryngol 2007;8:435–46.

[18] Robertson NG, Skvorak AB, Yin Y, Weremowicz S, Johnson KR, Kovatch KA, et al. Mapping and characterization of a novel cochlear gene in human and in mouse: a positional candidate gene for a deafness disorder, DFNA9. Genomics 1997;46:345–54.

[19] Robertson NG, Hamaker SA, Patriub V, Aster JC, Morton CC. Subcellular localisation, secretion, and post-translational processing of normal cochlin, and of mutants causing the sensorineural deafness and vestibular disorder, DFNA9. J Med Genet 2003;40:479–86.

[20] Yao J, Py BF, Zhu H, Bao J, Yuan J. Role of protein misfolding in DFNA9 hearing loss. J Biol Chem 2010;285: 14909–19.

International Journal of Pediatric Otorhinolaryngology 77 (2013) 228–232

Contents lists available at SciVerse ScienceDirect

International Journal of Pediatric Otorhinolaryngology

journal homepage: www.elsevier.com/locate/ijporl

High prevalence of inner-ear and/or internal auditory canal malformations in children with unilateral sensorineural hearing loss

Sawako Masuda [a,*], Satoko Usui [a], Tatsuo Matsunaga [b]

[a] Department of Otorhinolaryngology, Institute for Clinical Research, National Mie Hospital, Tsu, Mie, Japan
[b] Department of Otolaryngology, Laboratory of Auditory Disorders, National Institute of Sensory Organs, National Tokyo Medical Center, Tokyo, Japan

ARTICLE INFO

Article history:
Received 14 August 2012
Received in revised form 29 October 2012
Accepted 3 November 2012
Available online 30 November 2012

Keywords:
Unilateral sensorineural hearing loss
Temporal bone computed tomography
Malformation
Inner ear
Cochlear nerve canal
Internal auditory canal

ABSTRACT

Objective: Radiological and genetic examination has recently advanced for diagnosis of congenital hearing loss. The aim of this study was to elucidate the prevalence of inner-ear and/or internal auditory canal malformations in children with unilateral sensorineural hearing loss (USNHL) for better management of hearing loss and genetic and lifestyle counseling.

Methods: We conducted a retrospective study of charts and temporal bone computed tomography (CT) findings of 69 consecutive patients 0–15 years old with USNHL. In two cases, genetic examination was conducted.

Results: Of these patients, 66.7% had inner-ear and/or internal auditory canal malformations. The prevalence of malformations in infants (age <1 year) was 84.6%, which was significantly higher than that in children 1–15 years old (55.8%; $p < 0.01$). Almost half of the patients (32; 46.4%) had cochlear nerve canal stenosis; 13 of them had cochlear nerve canal stenosis alone, and in 19 it accompanied other malformations. Internal auditory canal malformations were observed in 22 subjects (31.8%), 14 (20.3%) had cochlear malformations, and 5 (7.2%) had vestibular/semicircular canal malformations. These anomalies were seen only in the affected ear, except in two of five patients with vestibular and/or semicircular canal malformations. Two patients (2.9%) had bilateral enlarged vestibular aqueducts. Mutations were found in *SLC26A4* in one of the two patients with bilateral large vestibular aqueducts. The prevalence of a narrow internal auditory canal was significantly higher in subjects with cochlear nerve canal stenosis (50.0%) than in subjects with normal cochlear nerve canals (11.1%; $p < 0.01$). There were no correlations between the type and number of malformations and hearing level.

Conclusions: The prevalence of inner-ear and/or internal auditory canal malformations detected by high-resolution temporal bone CT in children with USNHL was very high. Radiological and genetic examination provided important information to consider the pathogenesis and management of hearing loss. Temporal bone CT should be recommended to children with USNHL early in life. *SLC26A4* mutation also should be examined in cases with bilateral enlarged vestibular aqueduct.

1. Introduction

Abnormalities of the temporal bone have been associated with congenital sensorineural hearing loss (SNHL) since reported by Mondini in 1791 [1]. However, most cases of congenital SNHL were believed to be caused by abnormalities of the membranous labyrinth that could not be detected by conventional imaging techniques [2,3]. Conventional computed tomography (CT) could identify congenital cochlear malformations such as complete labyrinthine aplasia (Michel deformity), a common cavity, cochlear aplasia/hypoplasia, and incomplete partition [2–4]. Because of improvements in high-resolution CT techniques, previously unrecognized bony abnormalities—including a large vestibular aqueduct, wide and stenotic internal auditory canal (IAC), and cochlear nerve canal (CNC) stenosis—have been reported [3,5]. Currently, abnormalities found by imaging techniques not only provide diagnostic information but also aid in genetic and lifestyle counseling [1] and guide clinicians to better management of hearing loss [6].

The aim of this study was to elucidate the prevalence of inner-ear and/or IAC malformations in children with unilateral SNHL (USNHL).

* Corresponding author at: Department of Otorhinolaryngology, National Mie Hospital, 357 Osato-Kubota, Tsu, Mie 514-0125, Japan. Tel.: +81 59 232 2531; fax: +81 59 232 5994.
E-mail address: masudas@mie-m.hosp.go.jp (S. Masuda).

0165-5876/$ – see front matter © 2012 Elsevier Ireland Ltd. All rights reserved.
http://dx.doi.org/10.1016/j.ijporl.2012.11.001

2. Patients and methods

We conducted a retrospective study of charts and temporal bone CT findings of consecutive USNHL patients 0–15 years old who were seen in the Department of Otorhinolaryngology of National Mie Hospital between January 2008 and December 2011. All procedures were approved by the Ethics Review Committee of National Mie Hospital.

2.1. Subjects

The study included 69 patients. USNHL was defined as a hearing threshold greater than 30 dB hearing level for at least one frequency (500–2000 Hz). Of the 69 patients, 32 were male and 37 were female. Their ages of diagnosis ranged from 0 to 15 years (mean ± 1 SD: 4.3 ± 6.7 years, median: 4 years). The distribution of age was shown in Fig. S1. Twenty-six (37.3% of the subjects) were infants less than 1 year old. Twenty-two children had failed newborn hearing screening (NBHL) in unilateral ear and 21 of them identified USNHL in 1 year of age. One boy who had failed NBHL first visited ENT clinic and diagnosed USNHL at the age of 3 years. There was neither subjects who passed NBHL nor ones who suspected progressive hearing loss before their diagnosis. One subject had Down's syndrome and one had tetralogy of Fallot. Patients with middle ear diseases and abnormalities, conductive and combined hearing loss revealed by pure-tone audiometry, and obvious acquired hearing loss were excluded from the study.

Supplementary material related to this article found, in the online version, at http://dx.doi.org/10.1016/j.ijporl.2012.11.001.

2.2. Audiometric evaluations

Severity of hearing loss was defined from the pure-tone average as follows: hearing level of 21–40 dB, mild; 41–70 dB, moderate; 71–95 dB, severe; and greater than 95 dB, profound [7]. Pure-tone average was defined as the average hearing threshold at 500, 1000, and 2000 Hz. Thirty-four patients in this study were too young to be examined with pure-tone audiometry initially; for these patients, USNHL was determined on the basis of auditory brainstem response (ABR) and auditory steady state response (ASSR) using an Audera® system (Grason-Stadler). Distortion product otoacoustic emissions (DPOAE) and tympanometry were performed for all subjects.

2.3. Evaluation of temporal bone CT findings

All the patients underwent high-resolution CT of temporal bone using a single-slice helical CT (HiSpeed DX/i, GE Healthcare Japan Ltd., Tokyo Hino, Japan). Contiguous 1 mm-thick sections parallel to the infraorbitomeatal line were acquired through the temporal bone, with a field of view of 230 mm, matrix size of 512 × 512, in-plane pixel size of 0.45 mm × 0.45 mm, tube voltage of 120 kV, tube current of 150 mAs and a reconstruction kernel for bone.

CT results for each patient were examined by two otologists who did not know which ear had hearing loss. Classification of inner-ear and IAC malformations was based on Sennaroglu's classification [4] and modified as follows:

1. Cochlear malformations: Michel deformity, cochlear aplasia, common cavity deformity, cochlear hypoplasia, incomplete partition type I (IP-I), incomplete partition type II (IP-II: Mondini deformity).
2. Vestibular/semicircular canal malformations: absent vestibule, hypoplastic vestibule, dilated vestibule/absent semicircular canal, hypoplastic semicircular canal, enlarged semicircular canal.
3. IAC malformations: absent, narrow, enlarged.
4. Vestibular aqueduct finding: large.
5. CNC finding: stenosis.

We defined IAC as narrow when the diameter at the level of the porous of the IAC was less than 3 mm or 2 mm smaller than the normal side and as wide when greater than 10 mm. A large vestibular aqueduct was defined as being greater than 1.5 mm at the midpoint of the vestibular aqueduct on axial images [8]. The width of the CNC was measured at its midportion. The measurements were manually obtained using calipers [5]. CNC stenosis was defined as when the width was less than 1.5 mm [9]. An example of CNC stenosis in the right ear is shown in Fig. 1.

2.4. Genetic examinations

Patients with large vestibular aqueducts participated in genetic examination. Blood samples were obtained from the proband and his/her parents. DNA was extracted from blood samples using the Gentra Puregene DNA isolation kit (Qiagen, Hamburg, Germany), and primers specific for *SLC26A4* (GenBank NG_008489) were designed. Primer sequences for *SLC26A4* are listed in Table S1, supporting information. Screening for *SLC26A4* mutations was performed by bidirectional sequencing of amplicons generated by PCR amplification of each exon (exons 1–21) and splice sites using an Applied Biosystems 3730 DNA Analyzer (Applied Biosystems, Foster City, CA, USA) and analyzed by SeqScape v2.6 (Applied Biosystems). Examinations were conducted only after written informed consent had been obtained from each individual or parents of the patients.

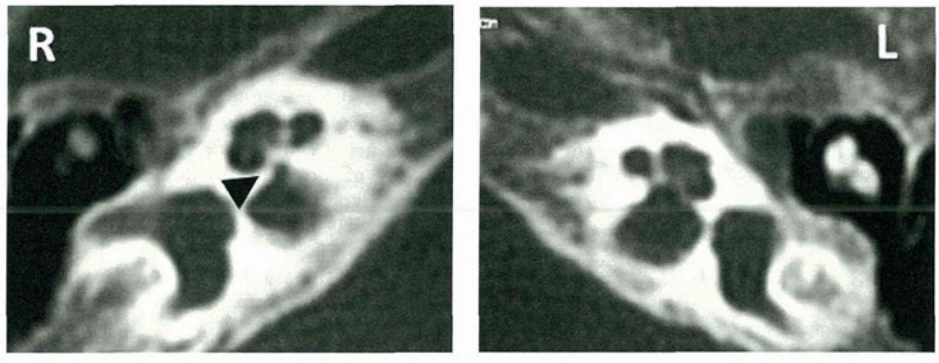

Fig. 1. Cochlear nerve canal stenosis demonstrated by transverse, thin-section CT scan of the temporal bone in three-month old boy. The left panel shows the hearing-impaired right ear (R), and the right panel shows the normal left ear (L). The arrowhead indicates the stenotic cochlear nerve canal in the right ear.

Supplementary material related to this article found, in the online version, at http://dx.doi.org/10.1016/j.ijporl.2012.11.001.

2.5. Statistical analysis

The significance of the prevalence of the inner-ear and/or IAC malformations between infants younger than 1 year of age and children from 1 to 15 years of age, and the association between the existence of malformations and hearing level was determined by the χ^2 test.

3. Results

The prevalence of inner-ear and/or IAC malformations is shown in Fig. 2. Of the 69 subjects, 66.7% had malformations. The prevalence of malformations in infants younger than 1 year of age (84.6%) was significantly higher than that in children 1–15 years of age (55.8%; $p < 0.01$).

Table 1 shows the prevalence of each malformation. The most common anomaly was CNC stenosis of the affected ear, seen in 46.4% of the subjects. Next in frequency were IAC malformations, followed by cochlear malformations and vestibular and/or semicircular canal malformations. These anomalies were seen in the affected ear alone, except for two of five patients with vestibular and/or semicircular canal malformations. Two patients had bilateral enlarged vestibular aqueducts.

The combination of malformations we observed is summarized in Table 2. Of the 69 patients, 13 (18.8%) had CNC stenosis alone, 19 (27.5%) had CNC stenosis accompanied with other malformations, and 4 (5.8%) had narrow IAC alone. Two patients with bilateral enlarged vestibular aqueducts had cochlear or cochlear and vestibular/semicircular canal malformations. In both cases, unilateral hearing loss was found by newborn hearing screening. In one case, a 4-month-old boy, genetic examination identified a compound heterozygous mutation [p.T410M (c.1229C>T)/p.L743X (c.2228T>A)] in *SLC26A4* (Fig. S2). p.T410M was previously reported as a missense mutation [10] and p.L743X was previously reported as a nonsense mutation [11]. This nonsense substitution truncates the protein at codon 743, which is 38 amino acids from the end of the protein. This case was confirmed as Pendred syndrome. The hearing loss in his normal hearing ear developed at 1 year of age. In another case, a 2-month-old girl, pathological mutations were not found in *SLC26A4*. Her hearing level has been stable for 3 years.

Supplementary material related to this article found, in the online version, at http://dx.doi.org/10.1016/j.ijporl.2012.11.001.

Table 3 shows the relationship between CNC malformations and IAC malformations. Of 32 cases of CNC stenosis, 16 (50.0%) were comorbid with narrow IAC. In 36 subjects with normal CNC, 4 (11.1%) had narrow IAC. The prevalence of narrow IAC was significantly higher in subjects with CNC stenosis than in subjects with normal CNC ($p < 0.01$).

Table 4 shows the combination of malformations and hearing level. There were 6 cases of mild hearing loss, 13 cases of moderate hearing loss, 7 cases of severe hearing loss, and 43 cases of profound hearing loss. DPOAE was absent in the affected ear in all subjects, except for two patients with unilateral profound hearing loss with CNC stenosis and narrow IAC without cochlear/vestibular/semicircular canal malformations. These two patients demonstrated normal responses in DPOAE in both ears. In one of these cases, ABR was performed. The threshold of wave V was 95 dBnHL (normal Hearing Level) in the affected ear and 20 dBnHL in the normal ear. This case was confirmed as unilateral auditory

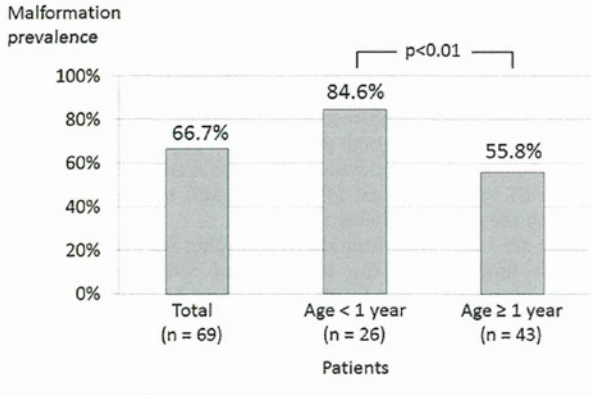

Fig. 2. Prevalence of inner-ear and/or internal auditory canal malformations found by temporal bone computed tomography.

Table 1
Prevalence of each malformation.

Malformation	Number (prevalence)
Cochlea	14 (20.3%)
Cochlear aplasia	0
Common cavity deformity	2 (2.9%)
Cochlear hypoplasia	1 (1.4%)
Incomplete partition (IP-I, IP-II)	11 (15.9%)
Vestibular/semicircular canal	5[a] (7.2%)
Internal auditory canal	22 (31.8%)
Narrow	20 (29.0%)
Enlarged	1 (1.4%)
Absent	1 (1.4%)
Vestibular aqueduct: enlarged (bilateral)	2 (2.9%)
Cochlear nerve canal: stenosis	32 (46.4%)

[a] Two cases had malformation in both ears.

Table 2
Combination of malformations.

Combination of malformations	Number (percentage)
CNC stenosis	13 (18.8)
CNC stenosis + narrow IAC	10 (14.5)
CNC stenosis + narrow IAC + C malformations	5 (7.2)
CNC stenosis + narrow IAC + V/SC malformations	1[a] (1.4)
CNC stenosis + C malformations	3 (4.3)
Narrow IAC	4 (5.8)
Large IAC	1 (1.4)
C malformations	2 (2.9)
C/V/SC malformations	2 (2.9)
V/SC malformations	2[b] (2.9)
Large VA + C malformations	1 (1.4)
Large VA + C malformations + V/SC malformations	1 (1.4)
CC with absent IAC	1 (1.4)
Normal	23 (33.3)
Total	69 (100.0)

CNC stenosis, cochlear nerve canal stenosis; IAC, internal auditory canal; C, Cochlear; V/SC, vestibular/semicircular canal; VA, vestibular aqueduct; CC: common cavity.
[a] This patient had bilateral V/SC malformations.
[b] One patient had bilateral V/SC malformations.

Table 3
Relationship between cochlear nerve canal malformations and internal auditory canal malformations.

Cochlear nerve canal		Internal auditory canal	
Stenosis	32 (46.4%)	Narrow	16 (50.0%)
		Normal	16 (50.0%)
Normal	36 (52.2%)	Narrow	4 (11.1%)
		Normal	31 (86.1%)
		Large	1 (2.8%)
Absent	1 (1.4%)	Absent	1 (100.0%)

Table 4
Combination of malformations and hearing level.

Cochlear nerve canal stenosis		+				−				Total
Narrow internal auditory canal		+		−		+		−		
Cochlear/vestibular/semicircular canal malformations		+	−	+	−	+	−	+	−	
Hearing level	Mild (21–40 dB)			1			1		4	6
	Moderate (41–70 dB)	1			3		1	4	4	13
	Severe (71–95 dB)	2			1			1	3	7
	Profound (>95 dB)	4[a]	10[b]	2	9		2	4	12	43
Total		7	10	3	13		4	9	23	69

[a] One patient had common cavity with IAC deficiency.
[b] Two patients demonstrated normal distortion product otoacoustic emissions.

neuropathy spectrum disorder. There were no correlations between the hearing level and the existence of CNC stenosis, narrow IAC, or other malformations in subjects with absence of DPOAE.

4. Discussion

The data in the present study showed a high prevalence of inner-ear and/or IAC malformations in pediatric USNHL. The prevalence was 84.6% in infants younger than 1 year of age. Most USNHL in these infants was considered as congenital, implying that more than 80% of the congenital USNHL was caused by morphological abnormality accompanied with bony anomalies.

The frequency of reported abnormal temporal bone findings in patients with USNHL varies from 7% to 44% [7]. Song et al. [8] studied CT of 322 children with USNHL and reported that 28.9% had malformations. Simons et al. [7] reported that the prevalence of CT abnormalities was 35% (29 of 83 cases), and the prevalence of magnetic resonance imaging (MRI) abnormalities was 25% (10 of 40 cases) in children with USNHL. However, they did not refer to the CNC.

The size of the CNC was first reported by Fatterpekar et al. in 2000 [5]. They demonstrated that the length and width of the CNC were significantly smaller ($p < 0.05$) in patients with congenital SNHL who had "normal" findings at thin-section temporal bone CT than in the control group. In 2008, Kono [3] investigated 118 patients without inner-ear malformations among 160 patients with USNHL, and 60% showed a significant difference in the CNC diameters between the affected and unaffected sides. Kono suggested that a diameter of less than 1.7 mm on transverse images or less than 1.8 mm on coronal images was hypoplasia. Stjernholm et al. [12] suggested that if the CNC diameter was less than 1.4 mm, then the possibility of cochlear nerve abnormality should be considered. Recent studies [9,13] demonstrated that CNC stenosis with a diameter of 1.5 mm or less as assessed with CT suggested cochlear nerve deficiency or hypoplasia as assessed with MRI. Wilkins et al. [14] showed a significant correlation between the degree of CNC stenosis and the degree of hearing loss. In the present study with the definition that the diameter was less than 1.5 mm, 46.4% of the subjects had CNC stenosis.

The exact cause of narrow CNC is unclear. Proper development of the IAC requires the presence of a normal cochlear nerve as a stimulus for attaining normal adult dimensions [5]. There is a possibility that the normal development of the CNC similarly needs the nerve for stimulus [5,15]. Fatterpekar et al. [5] speculated that, in patients with abnormality involving the membranous labyrinth, inhibition of the normal trophic effects of nerve growth factors owing to a diminutive cochlear nerve results in a small CNC. That is to say, hypoplasia of the CNC might be secondary to a hypoplastic cochlear nerve associated with some abnormality of a membranous labyrinth that could not be detected by current imaging techniques [3]. Very few of our subjects demonstrated a positive response in DPOAE, suggesting that at least the outer hair cells were affected or may not exist in most patients with USNHL.

The abnormalities found by imaging techniques provide information for diagnosis, management of hearing loss, and genetic and lifestyle counseling [1,6]. Congenital malformed inner ears may be associated with cerebrospinal fluid leakage, and thus development of meningitis is a very real possibility. Parents of children with inner-ear anomalies should be informed of the early symptoms and signs of meningitis. Consideration also should be given to immunization against common organisms implicated in meningitis [16]. Genetic examination should be recommended for patients with enlarged vestibular aqueducts. Pourova et al. [17] recommend performing SLC26A4 mutation analysis, following GJB2 analysis, in all hearing loss patients with bilateral enlarged vestibular aqueduct and/or associated thyroid impairment. Thy also mentioned that it is not reasonable to test the SLC26A4 gene in children with sporadic deafness without knowledge of their temporal bone CT/MRI images or even with its normal result. Mutations in the SLC26A4 are responsible for Pendred syndrome [18] as well as DFNB4 (non-syndromic hearing loss with inner ear abnormalities—enlarged vestibular aqueduct and/or Mondini deformity) [19]. Pendred syndrome and bilateral enlarged vestibular aqueduct correlates with the presence of two mutant alleles of *SLC26A4* [17,20,21]. Hearing loss in most patients with *SLC26A4* mutations fluctuates and is progressive [22]. Mutations in *SLC26A4* indicate the necessity for careful management of hearing and comorbidities, such as goiter.

The lack of MRI examination is one of the limitations in the present study. The results suggest the importance of temporal bone CT. Nevertheless, the risks of sedation/anesthesia for imaging in infants and young children, or indeed the radiation risk should be considered. The ideal imaging algorithm in children with unilateral or asymmetric SNHL is controversial [7]. MRI can detect soft-tissue abnormalities such as cochlear nerve deficiency with normal CNC and IAC. Simons et al. [7] suggested that virtually all children with SNHL should have an imaging study as part of their workup. They prefer high-resolution temporal bone CT as the initial study because of a high prevalence of positive findings and less cumbersome logistical issues. They also recommended that a negative CT scan should be followed by MRI to rule out SNHL caused by the central nervous system.

There are some other limitations regarding the current study. The first limitation is the diagnosis of SNHL. USNHL was determined on the basis of ABR and ASSR in 34 young patients. Middle-ear diseases and abnormalities were ruled out by CT and tympanometry; however, there is a possibility that some patients had conductive or combined hearing loss. Another limitation concerns the number of subjects. We examined 69 children, however, the evaluations should be need in the larger group.

In conclusion, a high prevalence of inner-ear and/or IAC malformations was detected by high-resolution temporal bone CT in children with USNHL. Radiological and genetic examination provided important information concerning the pathogenesis and management of hearing loss. The results of this study supported the recommendation of temporal bone CT to children with USNHL early in life. Genetic examination of *SLC26A4* also should be performed in all cases with bilateral enlarged vestibular aqueduct. The study in the larger group will likely refine the clinical protocol.

Acknowledgment

This research was supported by a Grant-in-Aid for Clinical Research from the National Hospital Organization, Tokyo, Japan.

References

[1] J.E. McClay, R. Tandy, K. Grundfast, S. Choi, G. Vezina, G. Zalzal, et al., Major and minor temporal bone abnormalities in children with and without congenital sensorineural hearing loss, Arch. Otolaryngol. Head Neck Surg. 128 (2002) 664–671.
[2] J.D. Swartz, H.R. Harnsberger, The otic capsule and otodystrophies, in: J.D. Swartz, H.R. Harnsberger (Eds.), Imaging of the Temporal Bone, 3rd ed., Thieme, New York, 1998, pp. P240–P266.
[3] T. Kono, Computed tomographic features of the bony canal of the cochlear nerve in pediatric patients with unilateral sensorineural hearing loss, Radiat. Med. 26 (2008) 115–119.
[4] L. Sennaroglu, I. Saatci, A new classification for cochleovestibular malformations, Laryngoscope 112 (2002) 2230–2241.
[5] G.M. Fatterpekar, S.K. Mukherji, J. Alley, Y. Lin, M. Castillo, Hypoplasia of the bony canal for the cochlear nerve in patients with congenital sensorineural hearing loss: initial observations, Radiology 215 (2000) 243–246.
[6] R.S. Yiin, P.H. Tang, T.Y. Tan, Review of congenital inner ear abnormalities on CT temporal bone, Br. J. Radiol. 84 (2011) 859–863.
[7] J.P. Simons, D.L. Mandell, E.M. Arjmand, Computed tomography and magnetic resonance imaging in pediatric unilateral and asymmetric sensorineural hearing loss, Arch. Otolaryngol. Head Neck Surg. 132 (2006) 186–192.
[8] J.J. Song, H.G. Choi, S.H. Oh, S.O. Chang, C.S. Kim, J.H. Lee, Unilateral sensorineural hearing loss in children: the importance of temporal bone computed tomography audiometric follow-up, Otol. Neurotol. 30 (2009) 604–608.
[9] M. Miyasaka, S. Nosaka, N. Morimoto, H. Taiji, H. Masaki, CT and MR imaging for pediatric cochlear implantation: emphasis on the relationship between the cochlear nerve canal and the cochlear nerve, Pediatr. Radiol. 40 (2010) 1509–1516.
[10] B. Coyle, W. Reardon, J.A. Herbrick, L.C. Tsui, E. Gausden, J. Lee, et al., Molecular analysis of the Pds gene in Pendred syndrome (sensorineural hearing loss and goitre), Hum. Mol. Genet. 7 (1998) 1105–1112.
[11] Y.Y. Yuan, P. Dai, Q.W. Zhu, D.Y. Kang, D.L. Huang, Sequencing analysis of whole SLC26A4 gene related to IVS7-2A>G mutation in 1552 moderate to profound sensorineural hearing loss patients in China, Zhonghua Er Bi Yan Hou Tou Jing Wai Ke Za Zhi 44 (2009) 449–454.
[12] C. Stjernholm, C. Muren, Dimensions of the cochlear nerve canal: a radioanatomic investigation, Acta Otolaryngol. 122 (2002) 43–48.
[13] S. Komatsubara, A. Haruta, Y. Nagano, T. Kodama, Evaluation of cochlear nerve imaging in severe congenital sensorineural hearing loss, ORL J. Otorhinolaryngol. Relat. Spec. 69 (2007) 198–202.
[14] A. Wilkins, S.P. Prabhu, L. Huang, P.B. Ogando, M.A. Kenna, Frequent association of cochlear nerve canal stenosis with pediatric sensorineural hearing loss, Arch. Otolaryngol. Head Neck Surg. 138 (2012) 383–388.
[15] J.W. Casselman, F.E. Offeciers, P.J. Govaerts, R. Kuhweide, H. Geldof, T. Somers, et al., Aplasia and hypoplasia of the vestibulocochlear nerve: diagnosis with MR imaging, Radiology 202 (1997) 773–781.
[16] P.G. Reilly, A.K. Lalwani, R.K. Jackler, Congenital anomalies of the inner ear, in: Pediatric Otology and Neurotology, Lippincott-Raven Publishers, Philadelphia, 1998, pp. 201–210.
[17] R. Pourová, P. Janousek, M. Jurovcík, M. Dvoráková, M. Malíková, D. Rasková, et al., Spectrum and frequency of SLC26A4 mutations among Czech patients with early hearing loss with and without Enlarged Vestibular Aqueduct (EVA), Ann. Hum. Genet. 74 (2010) 299–307.
[18] L.A. Everett, B. Glaser, J.C. Beck, J.R. Idol, A. Buchs, M. Heyman, et al., Pendred syndrome is caused by mutations in a putative sulphate transporter gene (PDS), Nat. Genet. 17 (1997) 411–422.
[19] S.P. Pryor, A.C. Madeo, J.C. Reynolds, N.J. Sarlis, K.S. Arnos, W.E. Nance, et al., SLC26A4/PDS genotype-phenotype correlation in hearing loss with enlargement of the vestibular aqueduct (EVA): evidence that Pendred syndrome and non-syndromic EVA are distinct clinical and genetic entities, J. Med. Genet. 42 (2005) 159–165.
[20] C.C. Wu, Y.C. Lu, P.J. Chen, P.L. Yeh, Y.N. Su, W.L. Hwu, et al., Phenotypic analyses and mutation screening of the SLC26A4 and FOXI1 genes in 101 Taiwanese families with bilateral nonsyndromic enlarged vestibular aqueduct (DFNB4) or Pendred syndrome, Audiol. Neurootol. 15 (2010) 57–66.
[21] T. Ito, B.Y. Choi, K.A. King, C.K. Zalewski, J. Muskett, P. Chattaraj, et al., SLC26A4 genotypes and phenotypes associated with enlargement of the vestibular aqueduct, Cell. Physiol. Biochem. 28 (2011) 545–552.
[22] H. Suzuki, A. Oshima, K. Tsukamoto, S. Abe, K. Kumakawa, K. Nagai, et al., Clinical characteristics and genotype–phenotype correlation of hearing loss patients with SLC26A4 mutations, Acta Otolaryngol. 127 (2007) 1292–1297.

Acta Oto-Laryngologica, 2012; Early Online, 1–7

informa
healthcare

ORIGINAL ARTICLE

Genetic analysis of *PAX3* for diagnosis of Waardenburg syndrome type I

TATSUO MATSUNAGA[1], HIDEKI MUTAI[1], KAZUNORI NAMBA[1], NORIKO MORITA[2] & SAWAKO MASUDA[3]

[1]*Department of Otolaryngology, Laboratory of Auditory Disorders, National Institute of Sensory Organs, National Tokyo Medical Center, Tokyo,* [2]*Department of Otolaryngology, Teikyo University School of Medicine, Tokyo and* [3]*Department of Otorhinolaryngology, Institute for Clinical Research, National Mie Hospital, Tsu, Japan*

Abstract

Conclusion: PAX3 genetic analysis increased the diagnostic accuracy for Waardenburg syndrome type I (WS1). Analysis of the three-dimensional (3D) structure of PAX3 helped verify the pathogenicity of a missense mutation, and multiple ligation-dependent probe amplification (MLPA) analysis of *PAX3* increased the sensitivity of genetic diagnosis in patients with WS1. *Objectives:* Clinical diagnosis of WS1 is often difficult in individual patients with isolated, mild, or non-specific symptoms. The objective of the present study was to facilitate the accurate diagnosis of WS1 through genetic analysis of *PAX3* and to expand the spectrum of known *PAX3* mutations. *Methods:* In two Japanese families with WS1, we conducted a clinical evaluation of symptoms and genetic analysis, which involved direct sequencing, MLPA analysis, quantitative PCR of *PAX3*, and analysis of the predicted 3D structure of PAX3. The normal-hearing control group comprised 92 subjects who had normal hearing according to pure tone audiometry. *Results:* In one family, direct sequencing of *PAX3* identified a heterozygous mutation, p. I59F. Analysis of PAX3 3D structures indicated that this mutation distorted the DNA-binding site of PAX3. In the other family, MLPA analysis and subsequent quantitative PCR detected a large, heterozygous deletion spanning 1759–2554 kb that eliminated 12–18 genes including a whole *PAX3* gene.

Keywords: *Mutation, MLPA, clinical diagnosis, hearing loss, dystopia canthorum, pigmentary disorder*

Introduction

Waardenburg syndrome (WS) is a hereditary auditory pigmentary disorder that is responsible for 1–3% of congenital deafness cases [1]. WS is classified into four types based on symptoms other than the auditory and pigmentary disorder. Type I WS (WS1) includes dystopia canthorum, and this feature distinguishes WS1 from type II WS. Type III WS is similar to WS1 but is associated with musculoskeletal anomalies of the upper limbs. Type IV WS is similar to type I but is associated with Hirschsprung disease. Diagnostic criteria for WS1 have been proposed [2]. The clinical features of WS1 demonstrate incomplete penetrance and highly varied expression [3,4], which makes diagnosis in individual patients challenging. For example, WS1 patients may present only one isolated symptom. Diagnosis of high nasal root and medial eyebrow flare can be difficult when they are mild. Hearing loss and early graying are relatively common in the general population and are not specific to WS1. Thus, the accuracy of WS1 diagnosis needs to be improved by the use of additional diagnostic procedures.

It is reported that more than 90% of patients with WS1 harbor point mutations in *PAX3* [5], and an additional 6% of WS1 patients harbor partial or complete *PAX3* deletions [6]. This high frequency of *PAX3* mutation in WS1 suggests that clinical diagnosis of WS1 could be facilitated by *PAX3* genetic analysis. To date, more than 80 *PAX3*

Correspondence: Tatsuo Matsunaga, Department of Otolaryngology, Laboratory of Auditory Disorders, National Institute of Sensory Organs, National Tokyo Medical Center, 2-5-1 Higashigaoka, Meguro, Tokyo, 152-8902, Japan. Tel: +81 3 3411 0111. Fax: +81 3 3412 9811. E-mail: matsunagatatsuo@kankakuki.go.jp

This study was presented at the annual meeting of the Collegium Oto-Rhino-Laryngologicum Amicitiae Sacrum, Rome, August 28, 2012.

(Received 19 September 2012; accepted 20 October 2012)

ISSN 0001-6489 print/ISSN 1651-2251 online
DOI: 10.3109/00016489.2012.744470

mutations are reported to be associated with WS1 [5]. A de novo paracentric inversion on chromosome 2 in a Japanese child with WS1 provided a clue for identification of *PAX3* in the distal part of chromosome 2 [7]. However, only a few *PAX3* mutations including the chromosomal inversion have been reported in Japanese patients with WS1 since then [8,9].

In the present study, we conducted *PAX3* genetic analysis to facilitate diagnosis of WS1 in two Japanese families. In one family, to verify the pathogenicity of an identified missense mutation, we analyzed the effect of the mutation on the three-dimensional (3D) structure of PAX3. In the other family, no mutations were identified by direct sequencing, so multiple ligation-dependent probe amplification (MLPA) analysis was used to search for large deletions in *PAX3* and thereby increase the sensitivity of genetic diagnosis.

Material and methods

Patients and control subjects

Two Japanese families with WS1 were included in the study. The diagnosis of WS1 was based on criteria proposed by the Waardenburg Consortium [2]. The normal-hearing controls comprised 92 subjects who had normal hearing according to pure tone audiometry. This study was approved by the institutional ethics review board at the National Tokyo Medical Center. Written informed consent was obtained from all subjects included in the study or from their parents.

Clinical evaluation

A comprehensive clinical history was taken from subjects who were examined at our hospitals or from their parents. During physical examination, special attention was given to the color of the skin, hair, and iris, and to other anomalies such as dystopia canthorum, medial eyebrow flare, limb abnormalities, and Hirschsprung disease. After otoscopic examination, behavioral audiometric testing was performed. The test protocol was selected according to the developmental age of the subject (conditioned orientation response audiometry, play audiometry, or conventional audiometric testing, from 125 to 8000 Hz), and testing was performed using a diagnostic audiometer in a soundproof room. Auditory brainstem response (ABR) and otoacoustic emission were also evaluated in some subjects.

Direct sequencing

Genomic DNA from the subjects was extracted from peripheral blood leukocytes using the Gentra Puregene® Blood kit (QIAGEN, Hamburg, Germany). Mutation screening of *PAX3* was performed by bidirectional sequencing of each exon (exons 1–11) together with the flanking intronic regions using an ABI 3730 Genetic Analyzer (Applied Biosystems, Foster City, CA, USA). Primer sequences for *PAX3* are listed in Table I. Mutation nomenclature is based on the genomic DNA sequence of [GenBank accession no. NG_011632.1], with the A of the translation initiation codon considered as +1. Nucleotide conservation between mammalian species was evaluated using ClustalW (http://www.ebi.ac.uk/Tools/msa/clustalw2/). PolyPhen-2 software (http://genetics.bwh.harvard.edu/pph2/) was used to predict the functional consequence(s) of each amino acid substitution.

MLPA

MLPA analysis was performed using an MLPA kit targeting *PAX3*, *MITF*, and *SOX10* (SALSA MLPA Kit P186-B1, MRC-Holland, Amsterdam, The Netherlands) according to the manufacturer's protocol. Exon-specific MLPA probes for exons 1–9 of *PAX3* and control probes were hybridized to genomic DNA from the subjects and normal controls and ligated with fluorescently labeled primers. A PCR reaction was then performed to amplify the hybridized probes. The amplified probes were fractionated on an ABI3130xl Genetic Analyzer (Applied Biosystems) and the peak patterns were evaluated using GeneMapper (Applied Biosystems).

Real-time PCR

To determine the length of each deleted genomic region, 100 ng of genomic DNA from the subjects and a normal control were subjected to quantitative PCR (Prism 7000, Applied Biosystems) using Power SYBR® Green Master Mix (Life Technologies, Carlsbad, CA, USA) and 12 sets of primers designed to amplify sequence-tagged sites on chromosome 2 (GenBank accession nos: RH46518, RH30035, RH66441, GDB603632, 1988, RH24952, RH47422, RH65573, RH26526, RH35885, RH16314, and RH92249).

Homology modeling of the PAX3 paired domain

The DNA-binding site of the paired domain of PAX3 was modeled using SWISS-MODEL [10] with the crystal structure of the PAX5 paired domain-DNA complex (PDB ID:1PDN_chain C) as the template because PAX3 and PAX5 are functionally and structurally similar [11]. The amino acid

Table I. Primer sequences for *PAX3*.

Exon 1	Forward	5′-TGTAAAACGACGGCCAGTAGAGCAGCGCGCTCCATTTG-3′
	Reverse	5′-CAGGAAACAGCTATGACCGCTCGCCGTGGCTCTCTGA-3′
Exon 2	Forward	5′-TGTAAAACGACGGCCAGTAAGAAGTGTCCAGGGCGCGT-3′
	Reverse	5′-CAGGAAACAGCTATGACCGGTCTGGGTCTGGGAGTCCG-3′
Exon 3	Forward	5′-TGTAAAACGACGGCCAGTTAAACGCTCTGCCTCCGCCT-3′
	Reverse	5′-CAGGAAACAGCTATGACCGGGATGTGTTCTGGTCTGCCC-3′
Exon 4	Forward	5′-TGTAAAACGACGGCCAGTAATGGCAACAGAGTGAGAGCTTCC-3′
	Reverse	5′-CAGGAAACAGCTATGACCAGGAGACACCCGCGAGCAGT-3′
Exon 5	Forward	5′-TGTAAAACGACGGCCAGTGGTGCCAGCACTCTAAGAACCCA-3′
	Reverse	5′-CAGGAAACAGCTATGACCGGTGATCTGACGGCAGCCAA-3′
Exon 6	Forward	5′-TGTAAAACGACGGCCAGTTGCATCCCTAGTAAAGGGCCA-3′
	Reverse	5′-CAGGAAACAGCTATGACCGGTGTCCATGGAAGACATTGGG-3′
Exon 7	Forward	5′-AACTATTATTTCATCAGTGAAATC-3′
	Reverse	5′-ATTCACTTGTATAAAATATCCACC-3′
Exon 8	Forward	5′-TGTAAAACGACGGCCAGTTGAAGCCAGTAGGAAGGGTGGA-3′
	Reverse	5′-CAGGAAACAGCTATGACCTGCAGGTTAAGAAACGCAGTTTGA-3′
Exon 9a	Forward	5′-TGTAAAACGACGGCCAGTTTGATACCGGCATGTGTGGC-3′
	Reverse	5′-CAGGAAACAGCTATGACCTGCAGTCAGATGTTATCGTCGGG-3′
Exon 9b	Forward	5′-TGTAAAACGACGGCCAGTCACAACTTTGTGTCCCTGGGATT-3′
	Reverse	5′-CAGGAAACAGCTATGACCGGGACTCCTGACCAACCACG-3′
Exon 10–11	Forward	5′-TGTAAAACGACGGCCAGTGCAAATGGAATGTTCTAGCTCCTCG-3′
	Reverse	5′-CAGGAAACAGCTATGACCGGTCAGCTCCAGGATCATATGGG-3′

sequences of the PAX3 and PAX5 paired domains were 79% homologous. The predicted PAX3 structure and the p.I59F mutation structure were superimposed on the backbone atoms of the PAX5 paired domain-DNA complex and displayed using the extensible visualization system, UCSF Chimera [12].

Results

In family 1, the proband, a 9-month-old male, was the first child of unrelated Japanese parents. Abnormal responses were found upon newborn hearing screening in the left ear, and left hearing loss was diagnosed by ABR. On physical examination, dystopia canthorum was noted, with a W-index of 2.77. The patient's mother also had dystopia canthorum, with a W-index of 2.68. She also had a history of early graying that started at age 16 years. She had not been diagnosed with WS1. According to the parents, 10 members of this family, including the proband and the mother, showed clinical features consistent with WS1 (Figure 1). ABR performed in the proband

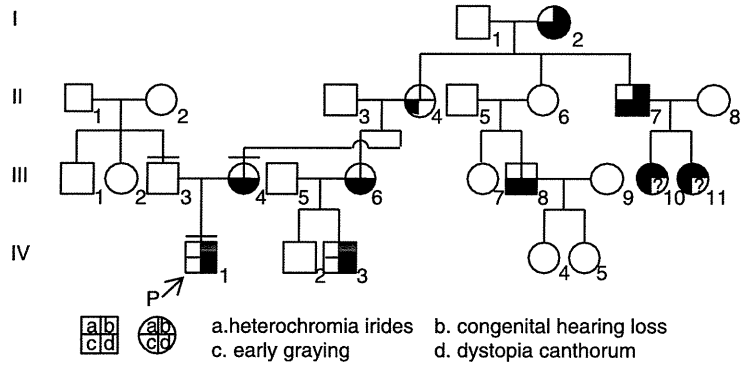

Figure 1. Pedigree of family 1. The proband is indicated by an arrow. The individuals we examined personally are indicated by a bar over the symbol. Phenotypes observed in this family are indicated symbolically as detailed below the pedigree.

revealed normal hearing in the right ear and no responses to 105 dB click stimuli in the left ear. Computed tomography (CT) of the temporal bone showed normal structures in the inner, middle, and outer ears.

Genetic analysis of *PAX3* was conducted in this family, and direct sequencing of *PAX3* revealed a heterozygous mutation, c.175A>T, in the proband and his mother. This mutation resulted in a missense mutation, p.I59F (Figure 2A). The proband's father did not harbor this mutation. p.I59F is located within exon 2 and is part of the paired domain of *PAX3*, which is a critical region for interaction between transcription factors and target DNA (Figure 2B). A multiple alignment of *PAX3* orthologs at this region demonstrated that I59 was evolutionarily conserved among various species (Figure 2C). The p.I59F mutation was not identified in any of the 184 alleles from the normal control subjects. This mutation was predicted to be 'probably damaging' according to PolyPhen-2 software.

The predicted 3D structures of the paired domain of the PAX3-DNA complex indicated that the PAX3 paired domain binds to the corresponding DNA (white double helixes) via hydrogen bonds (pink lines) at the N-terminal of α-helix1 (H1), α-helix2 (H2), and α-helix3 (H3) (indicated in blue; Figure 3A). I59 is located in the middle of H1, H2, and H3 and is surrounded by hydrophobic residues (green) protruding from H1, H2, and H3. Because the van der Waals radius of phenylalanine (Figure 3C; white arrows) is larger than that of isoleucine (Figure 3B, white arrowheads), F59 repels the surrounding hydrophobic residues by van der Waals forces and increases the distance between F59 and the surrounding hydrophobic residues, resulting in structural distortion of the DNA-binding site of PAX3. Since this site is precisely shaped for maximal binding to the corresponding DNA, this mutation is likely to reduce the binding ability of the paired domain of PAX3 and cause WSI. A mutational search found the same mutation in another Japanese family [8].

In family 2, the proband, a female aged 4 years and 4 months, was the first child of unrelated Japanese parents. Abnormal responses were found upon newborn hearing screening in the right ear, and right hearing loss was diagnosed by ABR. On physical examination, dystopia canthorum, medial eyebrow flare, and a white forelock were noted. She was admitted to hospital suffering from ketotic hypoglycemia of unknown cause when aged 4 years. Her mother presented with heterochromia iridis, dystopia canthorum, and medial eyebrow flare, and her grandmother presented with early graying that started at around 20 years of age, dystopia canthorum, and

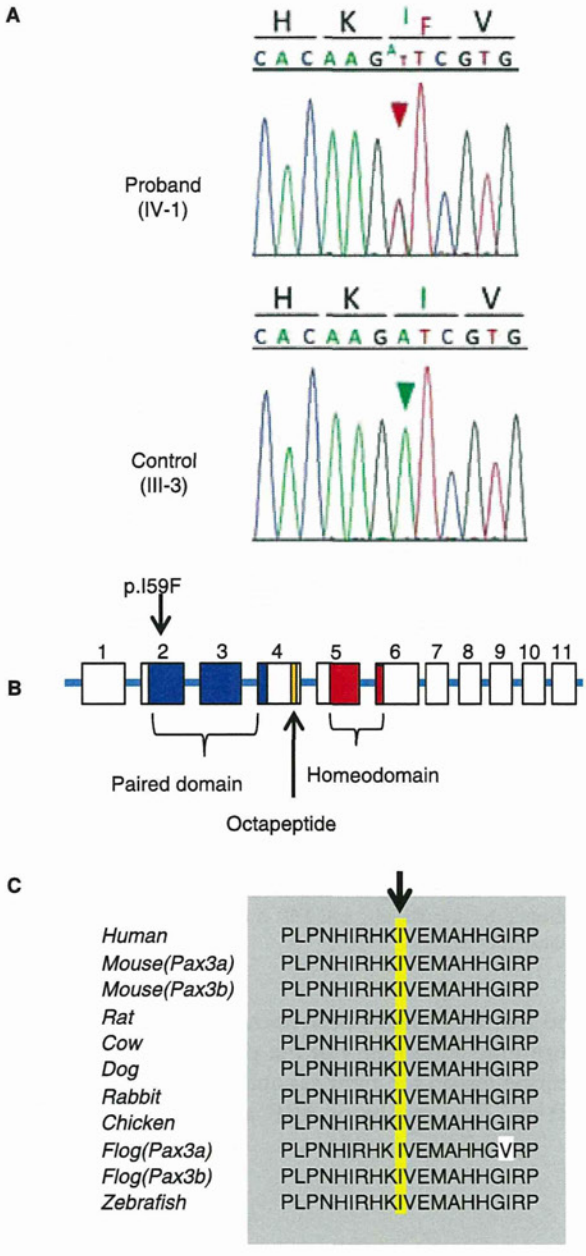

Figure 2. The p.I59F mutation of *PAX3* detected in family 1. (A) Sequence chromatogram for the proband and unaffected control. A heterozygous A to T transversion (red arrowhead) that changes codon 59 from ATC, encoding isoleucine (I), to TTC, encoding phenylalanine (F), was detected in the proband but not in the control (green arrowhead). (B) Localization of the p.I59F mutation and functional domains of PAX3. (C) A multiple alignment of PAX3 orthologs. Regions of amino acid sequence identity are shaded gray. The position of I59 is indicated by an arrow and shaded yellow.

medial eyebrow flare. According to the grandmother, the father of the grandmother also had dystopia canthorum and medial eyebrow flare. The pedigree of family 2 is shown in Figure 4. The grandmother

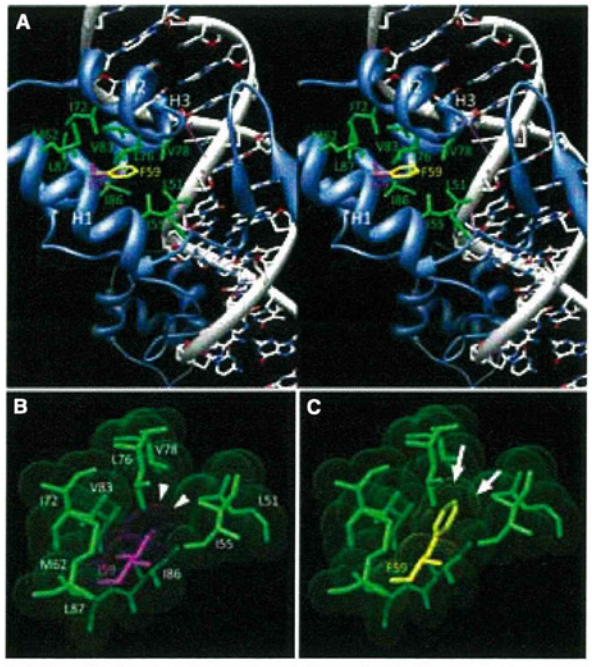

Figure 3. The predicted structure of the PAX3 paired domain-DNA complex. (A) The stereo view indicates that the mutated residue was surrounded by hydrophobic residues (green) protruding from H1, H2, and H3 of the paired domain (blue), which binds to DNA (white, sugar; blue, nitrogen; red, oxygen). The pink lines indicate hydrogen bonds. Magenta and yellow residues indicate I59 and F59, respectively. (B, C) The colored spheres indicate the van der Waals surface boundaries, the radius of the hydrophobic residues is shown in green, I59 is shown in magenta and is also indicated by arrowheads, and F59 is shown in yellow and is also indicated by arrows.

and her father had never been diagnosed with WS1. Pure tone audiometry of the proband showed severe hearing loss in the right ear and normal hearing in the left ear. The results of ABR and distortion product otoacoustic emissions in the proband were compatible with those obtained for pure tone audiometry.

Because direct sequencing of *PAX3* in the proband and her grandmother revealed no mutations, we conducted MLPA analysis to search for a large deletion of *PAX3*, and found that the copy number of all tested exons (exons 1–9) of *PAX3* was half that of the number of other chromosomal regions in both subjects (Figure 5A). In control subjects, all tested exons of *PAX3* showed the same copy number as the other chromosomal regions (Figure 5B). To determine the size of the deleted region, quantitative PCR was performed at 12 sequence-tagged sites on chromosome 2q36, which includes *PAX3*. In the proband, copy numbers at nine sites in the middle of the tested region (white arrows) were half that of those examined in normal controls, but the copy numbers at three of the sites near the 5' and 3' ends of the tested region (black arrows) were identical to those examined in normal controls (Figure 6). This result demonstrated that the chromosomal region spanning 1759–2554 kb at 2q36, which includes the whole *PAX3* gene, was deleted in one of the alleles of the proband. The same results were detected in the grandmother. A search for the deleted region revealed that this region contained between 12 and 18 genes, including *PAX3*.

Discussion

The heterozygous missense mutation, p.I59F, was identified in family 1. The pathogenicity of a novel or rare missense mutation in the causative gene is not necessarily verified even when the mutation is absent from a large number of normal controls, when the residue is evolutionary conserved among different species, or if the mutation is associated with the phenotype within a family, because an identified

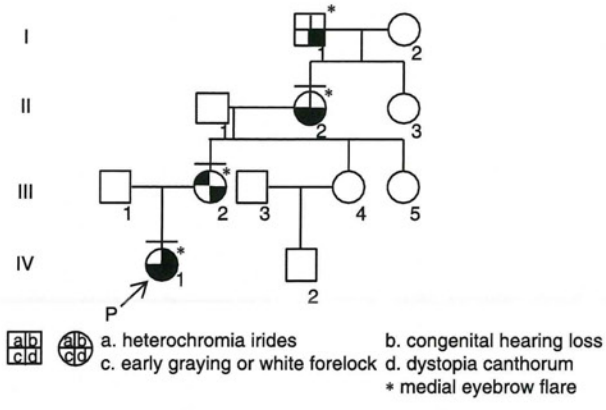

Figure 4. Pedigree of family 2. The proband is indicated by an arrow. The individuals we examined personally are indicated by a bar over the symbol. Phenotypes observed in this family are indicated symbolically, as detailed below the pedigree.